Bioorganic Chemistry 113 (2021) 104961

Contents lists available at ScienceDirect

Bioorganic Chemistry

journal homepage: www.elsevier.com/locate/bioorg

Discovery of new chalone adamantyl arotinoids having RXRα-modulating and anticancer activities

Mingtao Ao [1], Xianwen Hu [1], Yuqing Qian [1], Boqun Li, Jianyu Zhang, Yin Cao, Yuxiang Zhang, Kaiqiang Guo, Yingkun Qiu, Fuquan Jiang [*], Zhen Wu [*], Meijuan Fang [*]

Fujian Provincial Key Laboratory of Innovative Drug Target Research and State Key Laboratory of Cellular Stress Biology, School of Pharmaceutical Sciences and School of Chemistry and Chemical Engineering, Xiamen University, South Xiang-An Road, Xiamen 361102, China

ARTICLE INFO

Keywords:
Chalcone adamantly arotinoids
RXRα modulator
Apoptosis inducer
Antitumor
IKK

ABSTRACT

In the present study, a new series of chalcone adamantly arotinoids (chalcone AdArs) derived from RAR antagonist MX781, are synthesized, characterized, and evaluated for the biological activities *in vitro*. The studies of antiproliferative activity and RXRα-binding affinity of target compounds result in the discovery of a lead candidate (**WA15**), which is a good RXRα binder ($K_d = 2.89 \times 10^{-6}$ M) with potent antiproliferative activity against human cancer cell lines ($IC_{50} \approx 10$ μM) and low toxic to normal LO2 and MRC-5 cells ($IC_{50} > 50$ μM). Different from MX781, **WA15** eliminates RARα antagonist activity but inhibits 9-*cis*-RA-induced RXRα transactivation activity in a dose-dependent manner. Compound **WA15** is found to be a good apoptosis inducer in various cancer cells and promotes cell apoptosis in an RXRα-independent manner. Besides, **WA15** shows the induction of proteasome-dependent RXRα degradation which might enhance the **WA15**-induced apoptosis. Finally, the immunoblotting indicates that **WA15** can inhibit the TNFα-induced IKK activation and IκBα degradation, suggesting that the anticancer activity of **WA15** might be related to the inhibition of IKK/NF-κB signal pathway.

1. Introduction

Nuclear receptors (NRs) are ligand-activated transcription factors that play an important role in regulating multiple developmental, homeostatic, and metabolic processes by their genomic and non-genomic actions [1–7]. Aberrant expression and function of NRs are implicated in the development of many diseases such as fatty liver disease [8], neurodegenerative disease [9,10], and cancer [11–16]. Therefore, NRs have become important putative targets for drug development [17,18], leading pharmaceutical companies and research institutions to put efforts on developing the specific synthetic agonists or antagonists of NRs for disease treatment [19–21]. Among the NRs, retinoic acid receptors (RAR) and retinoid X receptor (RXR) have been studied for decades. Similar to other nuclear receptors, structurally they possess three main functional domains: a disordered *N*-terminal region, a DNA-binding domain, and a ligand-binding domain (LBD). A well-accepted mechanism for ligand-mediated nuclear receptor activities is that ligand binds to the ligand-binding pocket (LBP) to induce a major conformational change, converting the corepressor-binding site into a coactivator-binding site and triggering a cascade of events that lead to biological activities. Fig. 1 shows some ligands of RXR and RAR, which are constituted of three important aspects, including a polar motif head such as a carboxyl group, a central polyene linker, and a hydrophobic tail. 9-*cis* retinoic acid (9-*cis*-RA) is identified as an endogenous RXRα ligand (an agonist), while all-*trans* retinoic acid (ATRA) is an agonist of RARs that is used as a differentiation agent against acute promyelocytic leukemia [22,23]. Many synthetic modulators targeting RXRα or RAR are also developed [24–26]. For instance, a small synthetic molecule targeting RXRα, Targretin [27,28], acts as a highly effective agent for mammary carcinoma and is approved by FDA to treat cutaneous *T*-cell lymphoma [29]. Besides, many Retinoid-related molecules with an adamantyl group [30–32] are described with selective activities towards the retinoid receptors as RARβ/γ-selective agonist (CD437), RAR antagonists (MX781 and AHPC), or RXRα agonist (3-Cl-AHPC). Interestingly, the introduction of Cl in the RAR-selective ligand (AHPC) results in an RXR-selective ligand (3-Cl-AHPC). These AdArs have been found to

* Corresponding author.
E-mail addresses: jiangfq@xmu.edu.cn (F. Jiang), wuzhen@xmu.edu.cn (Z. Wu), fangmj@xmu.edu.cn (M. Fang).
[1] These authors contributed equally to this paper

https://doi.org/10.1016/j.bioorg.2021.104961
Received 14 September 2020; Received in revised form 21 April 2021; Accepted 1 May 2021
Available online 5 May 2021
0045-2068/© 2021 Elsevier Inc. All rights reserved.

induce apoptosis and inhibit cell growth in cancer cells as atypical retinoids or retinoid-related molecules (RRMs) [33,34]. RXR and RAR are attractive drug targets for anticancer therapy but their reported synthetic ligands including Targretin are limited in oncological therapeutic applications due to a variety of side effects. Thus, there is of great significance on exploring further structure–activity relations (SAR) of their reported ligands and discovering their novel small-molecule modulators with high efficacy and low toxicity.

Chalcones, which have a common 1,3-diaryl-2-propen-1-one chemical scaffold, are the core of many natural and synthetic compounds bearing wide-ranging biological activities such as anti-oxidant, antibacterial, antifungal, anti-inflammatory, and anti-tumor activities [35,36]. Today, chalcone appears to be an important structural skeleton in drug development, especially in the area of cancer therapy [37]. Among NRs modulators, MX781 is a chalcone adamantyl arotinoid which is first discovered as a RAR antagonist and significantly inhibits TNFα-mediated activation of IKK in various cancer cell lines [32,38]. Considering that recent studies of chalcone AdArs have not explored the effect of exchanging key functional groups of A and B phenyl rings such as carboxyl and adamantyl (Ad) groups on bioactivities, we herein report the synthesis of a new series of chalcone derivatives structurally related to MX781 along with their biological characterization to explore the further SAR of chalcone AdArs.

In this paper, 24 chalcone derivatives were synthesized and characterized. Among all synthesized chalcone derivatives, **WA15** displayed the most potent antiproliferative activities against HepG2 and A549 cancer cell lines (Table 1). Furthermore, **WA15** exhibited pan cytotoxicity against different cancer cell lines ($IC_{50} \approx 10$ μM) but low cytotoxic property in human normal cell lines (MRC-5 and LO2, $IC_{50} > 50$ μM). So **WA15**, as a representative compound, was evaluated the RARα/RXRα transactivation activity and the molecular basis of anticancer activity. It was found that **WA15** inhibited the transcription of RXRα in a concentration-dependent manner but had no effect on RARα transcriptional activity. The surface plasmon resonance (SPR) and isothermal titration calorimetry (ITC) assays showed that **WA15** has a good binding affinity with RXRα-LBD and the molecular docking study predicted the binding nature of **WA15** to RXRα with antagonistic conformation. Further bioassay showed that **WA15** showed apoptosis induction in the various tumor cell lines. **WA15** might induce the proteasome-dependent RXRα degradation to enhance the apoptosis induction as well as lead to cell death through inhibiting IKK/NF-κB signaling to result in cell death. Taken together, we found that the chalcone AdAr **WA15** was a new

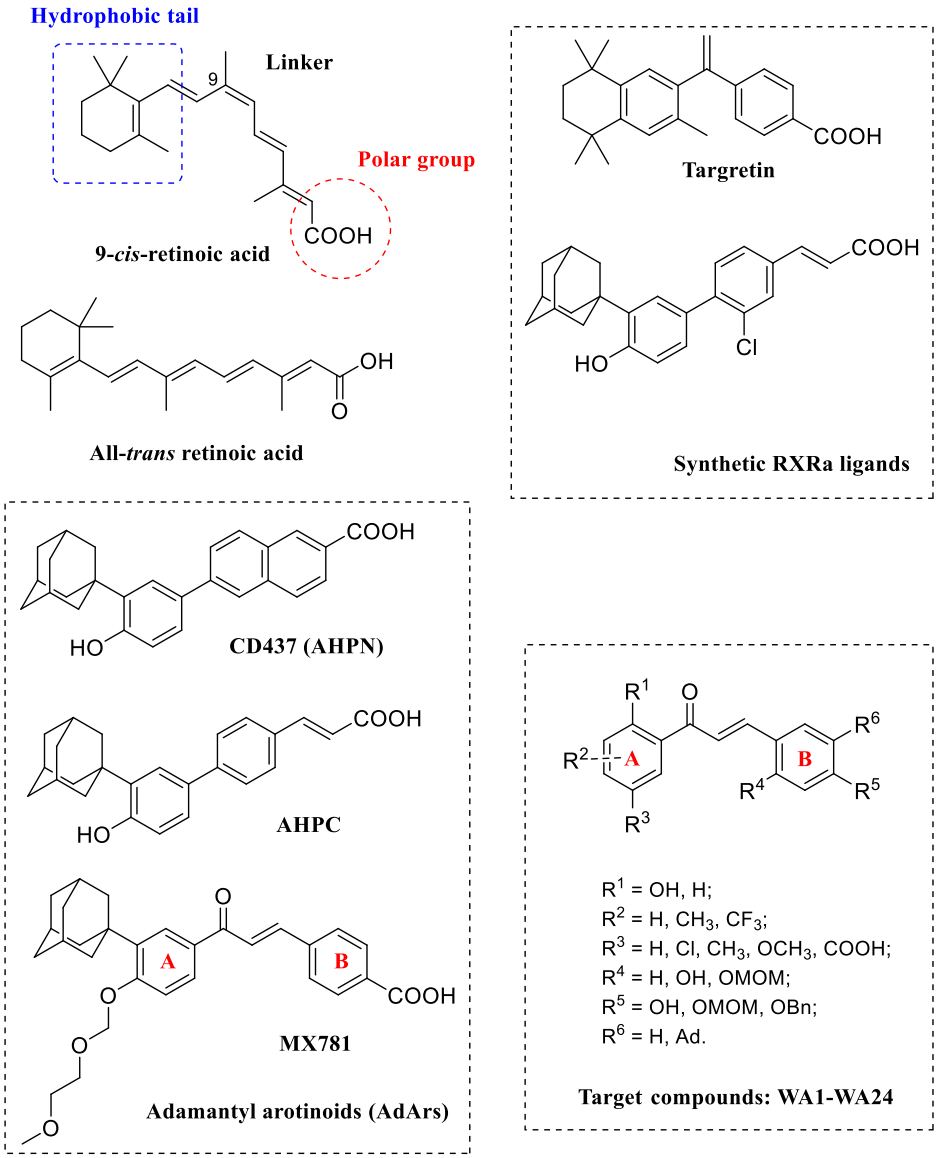

Fig. 1. Structures of selected retinoid-related molecules (RRMs) and target compounds.

Table 1
In vitro antiproliferative activities of target compounds against cancer HepG2 and A549 cells.

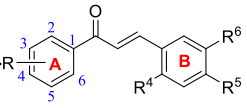

Comp.	R	R^4	R^5	R^6	IC_{50} (μM)[a]	
					HepG2	A549
MX781	3-Ad-4-MEM	H	COOH	H	4.27 ± 0.15	5.35 ± 0.21
WA1	2-OH	H	OCH_2OCH_3	Ad	45.65 ± 1.28	>50
WA2	2-OH-5-Cl	H	OCH_2OCH_3	Ad	27.15 ± 1.02	23.73 ± 0.71
WA3	2-OH-5-CH_3	H	OCH_2OCH_3	Ad	43.42 ± 1.18	42.26 ± 1.58
WA4	2-OH-5-OCH_3	H	OCH_2OCH_3	Ad	>50	>50
WA5	2-OH-5-COOH	H	OCH_2OCH_3	Ad	22.55 ± 0.71	12.08 ± 0.16
WA6	2-OH	H	OCH_2Ph	Ad	>50	>50
WA7	2-OH-5-Cl	H	OCH_2Ph	Ad	45.09 ± 1.27	37.69 ± 0.76
WA8	2-OH-5-CH_3	H	OCH_2Ph	Ad	>50	>50
WA9	2-OH-5-OCH_3	H	OCH_2Ph	Ad	>50	>50
WA10	2-OH-5-COOH	H	OCH_2Ph	Ad	28.57 ± 0.88	34.08 ± 1.09
WA11	2-OH	OCH_2OCH_3	OCH_2OCH_3	Ad	>50	>50
WA12	2-OH-5-Cl	OCH_2OCH_3	OCH_2OCH_3	Ad	48.17 ± 0.75	>50
WA13	2-OH-5-CH_3	OCH_2OCH_3	OCH_2OCH_3	Ad	>50	>50
WA14	2-OH-5-OCH_3	OCH_2OCH_3	OCH_2OCH_3	Ad	>50	>50
WA15	**2-OH-5-COOH**	**OCH_2OCH_3**	**OCH_2OCH_3**	**Ad**	**10.05 ± 0.16**	**9.30 ± 0.12**
WA16	3-CH_3	OCH_2OCH_3	OCH_2OCH_3	Ad	>50	>50
WA17	4-CH_3	OCH2OCH3	OCH_2OCH_3	Ad	>50	>50
WA18	3-CF_3	OCH_2OCH_3	OCH_2OCH_3	Ad	>50	>50
WA19	2-OH	H	OH	Ad	11.87 ± 0.21	25.54 ± 0.38
WA20	2-OH-5-Cl	H	OH	Ad	20.64 ± 0.68	26.45 ± 1.14
WA21	2-OH-5-CH_3	H	OH	Ad	40.60 ± 1.75	35.64 ± 0.17
WA22	2-OH-5-OCH_3	H	OH	Ad	20.22 ± 0.28	16.67 ± 1.41
WA23	2-OH-5-COOH	H	OH	Ad	22.78 ± 0.31	21.76 ± 1.12
WA24	2-OH-5-COOH	H	OH	H	>50	>50

[a] Data are means ± SD of triplicate experiments.

RXRα modulator and could act as a lead compound for anticancer therapy.

2. Results and discussion

2.1. Chemistry

The syntheses of Adamantly-substituted chalcones were carried out as shown in Scheme 1 (**WA1-WA18**) and Scheme 2 (**WA19-WA24**). Adamantly-substituted hydroxybenzaldehydes **2a** and **2b** were synthesized by Friedel-Crafts alkylation of hydroxybenzaldehydes **1a** and **1b** with adamantan-1-ol using sulfuric acid as catalyst, respectively. Then, **2a** and **2b** reacted with chloromethyl methyl ether (MOMCl) or benzyl bromide (BnBr), introducing the methoxymethyl (MOM) or benzyl (Bn) protecting group to get corresponding benzaldehydes **3a-3c**. 3-Acetyl-4-hydroxybenzoic acid (**6e**) was afforded by solvent-free Fries rearrangement of methyl 4-acetoxybenzoate **5** in the presence of $AlCl_3$. Aldol coupling reactions of acetophenones (**6a-6h**) with benzaldehydes (**3a-3c**) were performed in the presence of NaOH in MeOH at 70 °C, affording the adamantly-substituted chalcones **WA1-WA18**. As shown in Scheme 2, the removal of MOM protecting groups of **WA1-WA5** with 10% aqueous HCl in MeOH produced the corresponding target compounds **WA19-WA23**, while **WA24** without adamantyl substitution was synthesized from **6e** and 4-hydroxybenzaldehyde (**1a**) according to standard Claisen-Schmidt aldol condensation protocols. All target compounds were characterized by Nuclear Magnetic Resonance (^{1}H NMR and ^{13}C NMR), mass spectrometry (MS), and melting point (Mp).

2.2. Biological evaluation

2.2.1. In vitro antiproliferative activity

To explore the antitumor activity of these adamantyl chalcone derivatives, all compounds were first assayed for *in vitro* antiproliferative activities against HepG2, and A549 cancer cell lines using MTT assay with MX781 as a reference. The concentrations of compounds required for 50% inhibition of cell viability (IC_{50}) were determined and summarized in Table 1. The results indicated that more than half of the synthesized chalcone derivatives had antiproliferative activity against HepG2 and A549 cells with IC_{50} below 50 μM. Six compounds (**WA5**, **WA15**, **WA20**, **WA21**, **WA23**, and **WA24**) were active towards HepG2 cells (IC_{50} < 25 μM), two of which (**WA15** and **WA20**) exhibited promising cytotoxic activity (IC_{50} < 12 μM). The results listed in Table 1 implied that different substituted groups of the phenyl rings (ring-A and ring-B) had varied effects on the cell viability of HepG2 and A549 cells. So attempts were made to establish SAR among the tested compounds based on data collected from three independent experiments.

Using 3′-Ad-4′-MOMO substituents at ring-B and 2-OH substituent at ring-A, we examined the antiproliferative activities of compounds **WA1**, **WA2**, **WA3, WA4**, and **WA5** having H, CH_3, Cl, OCH_3, and COOH at C5′ position of ring-A, respectively. Among them, compound **WA5** with 5′-COOH group at ring-A exhibited the most excellent antiproliferative activity against the two tested cancer cell lines (HepG2 and A549). Meanwhile, **WA10** and **WA15** displayed lower IC_{50} values than **WA6-WA9** and **WA11-WA14**, respectively, indicating that **WA10** and **WA15** exhibited a similar SAR, with the carboxyl (COOH) group being the better substitution. A comparison of the activities of **WA1-WA5** and **WA6-WA10** showed that the 4′-OMOM substitution was better than 4′-OBn (IC_{50}: **WA2** < **WA7**, **WA3** < **WA8**, and **WA5** < **WA10**). Moreover, **WA15**, in which 2′-OMOM, 4′-OMOM, and 5′-Ad were simultaneously introduced to ring-B, showed the best antiproliferative activity.

When comparing 3′-Ad-4′-OH substituted derivatives (**WA19-WA23**) with 3′-Ad-4′-OMOM/3′-Ad-4′-OBn substituted derivatives (**WA1-WA5** and **WA6-WA10**), it was found that the replacement of the hydroxyl H atom by a methoxymethyl group or benzyl group for compounds bearing 3′,4′-disubstituted ring-B reduced antiproliferative activity. Additionally, all compounds containing no 2-OH on ring-A (**WA16-WA18**) showed a complete loss of antiproliferative activity. As for B-ring, the bulky adamantyl group seems to be necessary for antiproliferative activity, since compound **WA24** without the adamantyl substitution at position C4 of the B-ring had no activity with IC_{50} values up to 50 μM.

Next, compounds **WA5** and **WA15** which exerted good antiproliferative activity against HepG2 and A549 cells (IC_{50} < 15 μM) were selected to investigate their growth inhibition activity for another two lung cancer cell lines (H292 and H460) and two normal cell lines (LO2 and MRC-5). As depicted in Table 2, both **WA5** and **WA15** exhibited broad-spectrum antiproliferative activity against all tested four cancer lines. Notably, both **WA5** and **WA15** displayed lower cytotoxicity on human normal cells (LO2 and MRC-5) than the positive control MX781. Therefore, we took the most active compound **WA15** for further study.

2.2.2. The RAR/RXR transactivation profile of *WA15*

Based on the facts that the structures of synthetic RXRα/RXRγ LBD

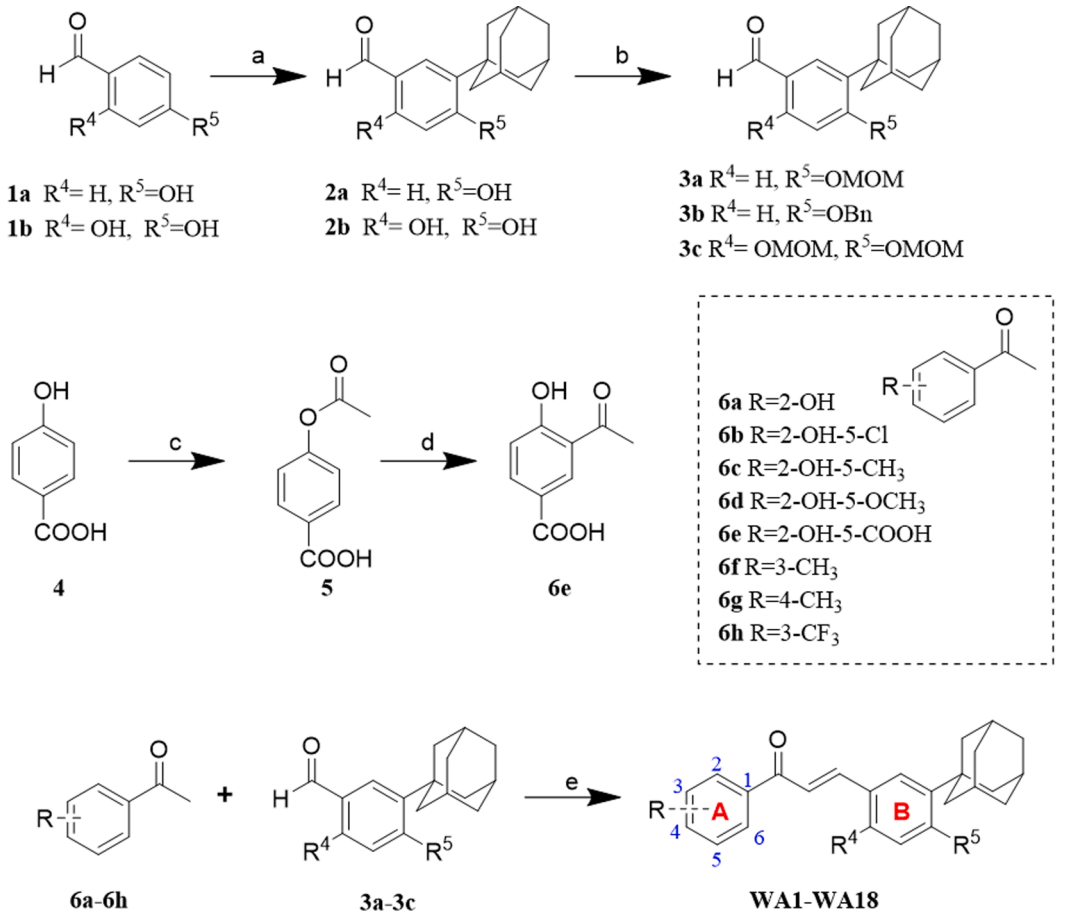

WA1 R=2-OH, R^4=H, R^5=OCH_2OCH_3
WA2 R=2-OH-5-Cl, R^4=H, R^5=OCH_2OCH_3
WA3 R=2-OH-5-CH_3, R^4=H, R^5=OCH_2OCH_3
WA4 R=2-OH-5-OCH_3, R^4=H, R^5=OCH_2OCH_3
WA5 R=2-OH-5-COOH, R^4=H, R^5=OCH_2OCH_3
WA6 R=2-OH, R^4=H, R^5=OCH_2Ph
WA7 R=2-OH-5-Cl, R^4=H, R^5=OCH_2Ph
WA8 R=2-OH-5-CH_3, R^4=H, R^5=OCH_2Ph
WA9 R=2-OH-5-OCH_3, R^4=H, R^5=OCH_2Ph
WA10 R=2-OH-5-COOH, R^4=H, R^5=OCH_2Ph
WA11 R=2-OH, R^4=R^5=OCH_2OCH_3
WA12 R=2-OH-5-Cl, R^4=R^5=OCH_2OCH_3
WA13 R=2-OH-5-CH_3, R^4=R^5=OCH_2OCH_3
WA14 R=2-OH-5-OCH_3, R^4=R^5=OCH_2OCH_3
WA15 R=2-OH-5-COOH, R^4=R^5=OCH_2OCH_3
WA16 R=3-CH_3, R^4=R^5=OCH_2OCH_3
WA17 R=4-CH_3, R^4=R^5=OCH_2OCH_3
WA18 R=3-CF_3, R^4=R^5=OCH_2OCH_3

Scheme 1. The synthesis of target compounds **WA1**-**WA18**. Reagents and conditions: (a) H_2SO_4, CH_2Cl_2, 45 °C, 16 h; (b) K_2CO_3, MOMCl or BnBr, acetone, 60 °C, 6 h; (c) Ac_2O, rt, 2 h; (d) $AlCl_3$, 160 °C, 5 h; (e) NaOH, MeOH, 70 °C, 16–20 h; (f) 10% aqueous HCl, MeOH, reflux, 1 h.

ligands are similar and micro-modifying RAR antagonists (CD437) can produce RXR-selective activators [30], herein we used transient transfections in HEK293T cells with expression vectors containing the Gal4 DNA binding domain fused to the C-terminus ligand-binding domain (LBD) of RARα or RXRα to evaluate the transactivation potential of the novel chalcone AdAr **WA15**. As shown in Fig. 2A and 2B, Gal4-RARα-LBD strongly activated the Gal4 reporter in the presence of the natural ligand all-*trans*-retinoic acid (ATRA), while Gal4-RXRα-LBD strongly activated the Gal4 reporter in the presence of 9-*cis*-RA. The RAR/RXR transactivation profile showed that neither **WA15** nor MX781 were capable of enhancing RAR- or RXR-driven luciferase activity when tested alone. Interestingly, the parental compound MX781 significantly inhibited ATRA-induced RARα transactivation as a RAR antagonist as previously reported, but **WA15** had little effect on the transcriptional activity of the Gal4–RARα fusion protein when tested at a high concentration of 10 μM in HEK-293 cells. Meanwhile, we observed that **WA15** elicited significant antagonistic activity against RXRα at the concentration of 10 μM but the parental compound MX781 was inactive against RXRα. Moreover, it was found that **WA15** possessed the dose-dependently inhibitory effect on the Gal4-DBD-RXRα-LBD transactivation induced by 9-*cis*-RA (Fig. 2C). These results implied that **WA15** was able to selectively interact with RXRα.

2.2.3. *Binding characterization of **WA15** to RXRα*

The regulation of RXRα transactivation by **WA15** prompted us to investigate the physical binding affinity of **WA15** toward the RXRα ligand-binding domain (LBD) *in vitro* using SPR and ITC assays. The SPR results (Fig. 3A) showed that **WA15** dose-dependently bound to RXRα-LBD with a dissociation constant (K_D) value of 2.31×10^{-6} M. Besides, the ITC assay further confirmed the binding of **WA15** to RXRα-LBD protein (Fig. 3B). The calculated K_D value from the ITC assay was 2.89×10^{-6} M, which was in the same order of magnitude as that measured by

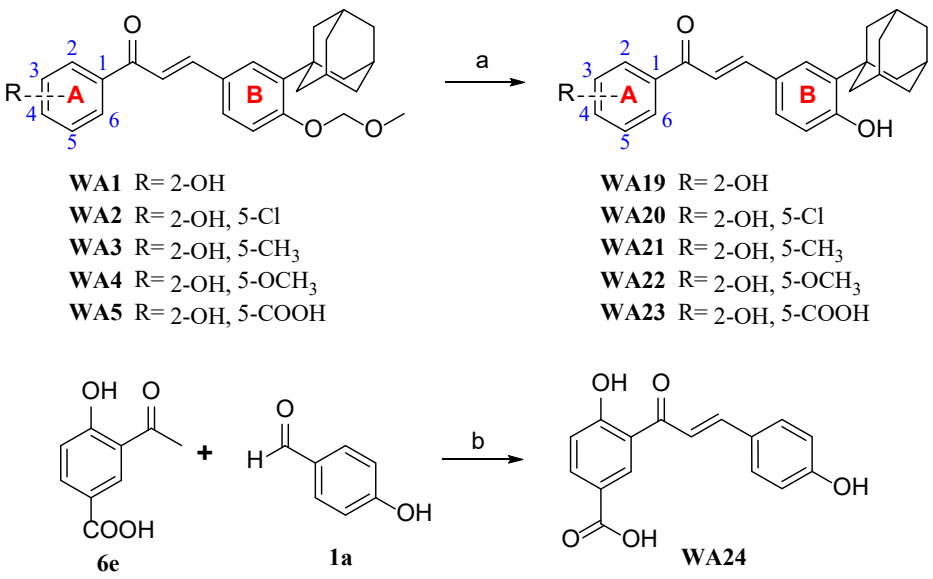

Scheme 2. The synthesis of target compounds **WA19-WA24**. Reagents and conditions: (a) 10% aqueous HCl, MeOH, reflux, 1 h; (b) NaOH, MeOH, 70 °C, 16–20 h.

Table 2
In vitro antiproliferative activities of selected compounds against cancer and normal cells.

Compd	IC_{50} (μmol/L)[a]					
	HepG2	A549	H460	H292	LO2	MRC-5
WA 5	22.55 ± 0.71	12.08 ± 0.16	12.19 ± 0.57	11.05 ± 0.31	>50	>50
WA 15	10.05 ± 0.16	9.30 ± 0.12	9.96 ± 0.29	9.01 ± 0.12	>50	>50
MX781	4.27 ± 0.15	5.35 ± 0.21	4.72 ± 0.07	3.84 ± 0.08	5.25 ± 0.48	6.75 ± 0.16

[a] Data are means ± SD of triplicate experiments.

the SPR assay. These data suggest that **WA15** is a good binder of RXRα. On the other hand, like other synthetic RXRα LBD ligands, the structure of **WA15** possesses three characteristic modules: adamantyl group as a hydrophobic moiety, a chalcone-based linker, and a carboxyl group as a polar moiety. Therefore, to examine the role of the carboxyl and adamantly groups for the binding activity of **WA15** to RXRα-LBD, we checked the physical binding affinity of synthesized compounds without carboxyl (**WA11**) or Ad (**WA24**) group to RXRα using SPR assay. The results showed that **WA11** and **WA25** could not bind to RXRα-LBD (Fig. 3A), indicating that the presence of both the carboxyl and the Ad groups was essential for the binding of **WA15** to RXRα.

Next, we performed molecular docking studies to evaluate the binding affinities and predict the binding model of selected compounds with an antagonistic conformation of RXRα (PDB: 3A9E, chain A) using Glide in XP mode. First, we docked the native ligand LG100754 back to the crystal structure of RXRα to validate the docking method. The re-docking pose of LG100754 obtained using Glide in XP mode overlaps well with its crystallized conformation with a root mean square deviation (RMSD) of 0.5262 Å, indicating that our docking protocol is reliable (Table S1 and Fig. S1). The docking scores of MX781, **WA15**, **WA11**, and **WA24** with RXRα-LBD are −9.181, −9.680, −7.363, and −7.904, respectively, while the native ligand LG100754 had a docking score of −11.936 (Table S1). The docking results indicated that **WA15** had a better binding affinity toward RXRα-LBD compared with MX781, **WA11**, and **WA24**. It is consistent with the results of the SPR assay. Therefore, the carboxyl and adamantly groups might be the important pharmacophores that induce the best binding conformation and interact with amino acid residues located in RXRα-LBP. Fig. 4 shows the hypothetical binding mode of the most potent chalone AdAr **WA15** in the LBP of RXRα. As shown in Fig. 4A, **WA15** is well docked into the RXRα-LBP. The binding features of **WA15** with RXRα are illustrated in Fig. 4B-4C. Similar to LG100754, the oxygen atom in the carboxyl group of phenyl ring-A of **WA15** forms a strong H-bond (distance: 1.83 Å) with ARG321 which is an important residue for the binding of RXRα antagonists to

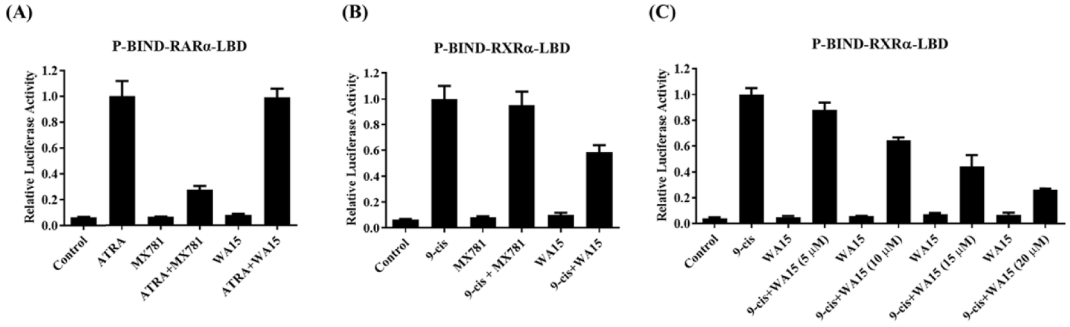

Fig. 2. The effect of **WA15** and MX781 on RARα/RXRα transactivation. (A) RARα transactivation profile. (B) RXRα transactivation profile. HEK293T cells co-transfected with p-BIND-RARα-LBD/RXRα-LBD and pG5-luc were treated with ATRA (0.1 μM), 9-*cis*-RA (0.1 μM), MX781 (5 μM), and **WA15** (10 μM) for 12 h, and luciferase activities were measured and normalized. (C) Dose-dependent effect of **WA15** on inhibiting RXRα transactivation. HEK293T cells co-transfected with pG5-Luc and p-Bind-RXRα-LBD were treated with 9-*cis*-RA (0.1 μM) alone or together with the indicated concentration of **WA15** for 12 h. Data shown are representative of at least three independent experiments.

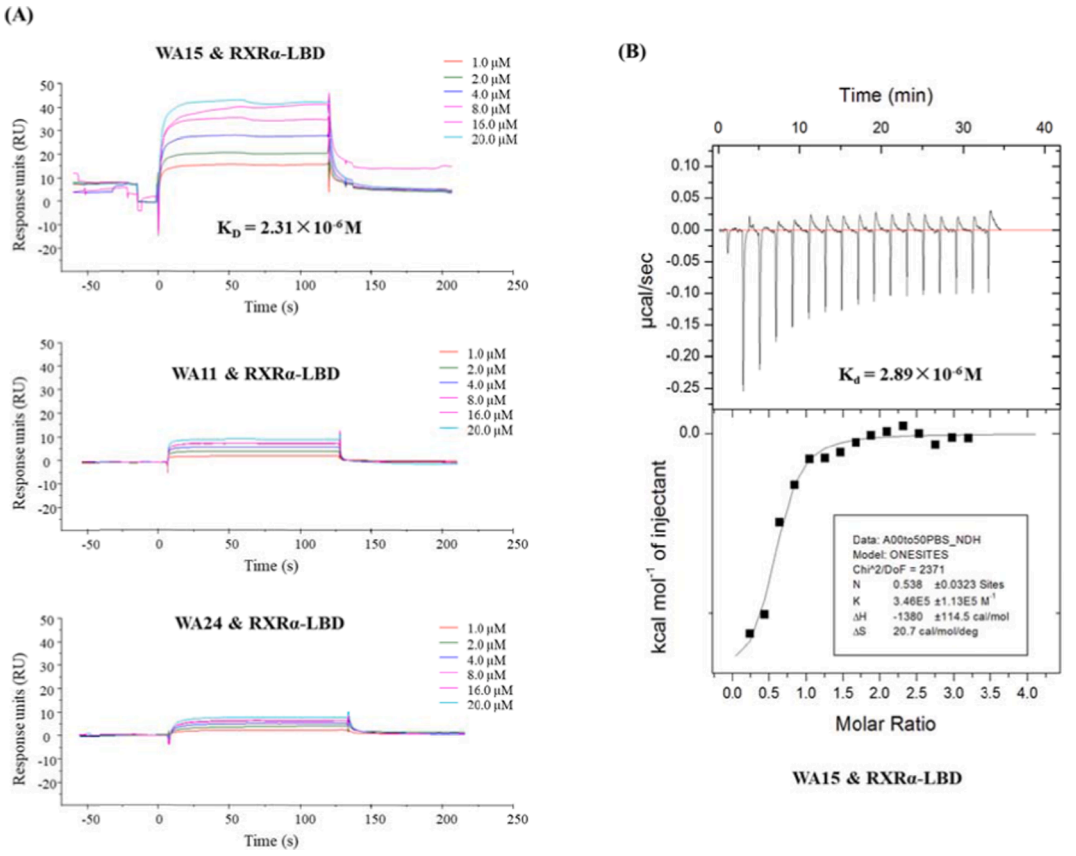

Fig. 3. The binding affinities of selected compounds toward RXRα-LBD. (A) The physical binding affinities of selected compounds to RXRα-LBD was evaluated by SPR assay. The sensorgrams were obtained from the injection of a series of concentrations of selected compounds over the immobilized RXRα-LBD chip. BIA evaluation software was used to determine the equilibrium dissociation constant (K_D). (B) The thermodynamic property of **WA15** binding to RXRα-LBD was investigated by ITC assay. The upper curve in the panel shows the measured heats for each injection, while the lower plot shows the enthalpies for each injection along with the fit to a single binding site model used to estimate the K_d.

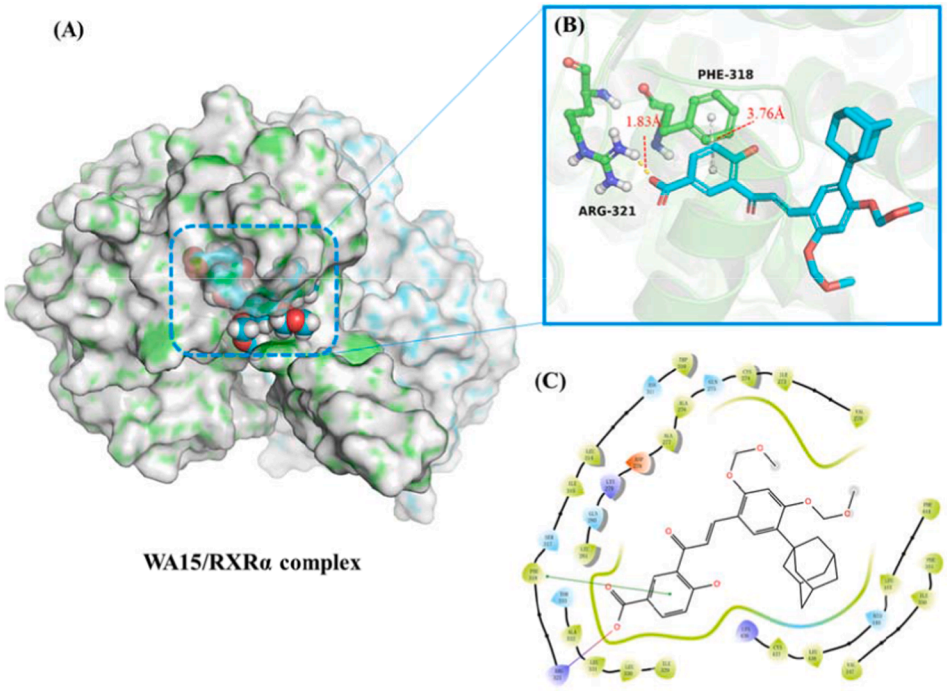

Fig. 4. The docking model of **WA15** into RXRα-LBD (3A9E). (A) Surface display of **WA15** (sphere) binding with RARα-LBD Pocket. (B) Close-up view depiction (3D model) of the superposition of **WA15** bound to RXRα-LBP. The RXRα binding site is presented with a green ribbon showing side chains of ARG321 and PHE318. W**A15** is shown in stick with cyan carbon and red oxygen. **WA15** engages in an H-bond interaction with ARG321 and a π-π stacking interaction with PHE318. (C) 2D binding model of **WA15** with RARα. Neighboring amino acids in colors were displayed in lines within a distance of 5 Å approximately to **WA15** (the hydrogen bond and π-π stacking interactions between **WA15** and RARα are shown as lines). The green color denotes the hydrophobic nature of amino acids, the red color denotes the acid amino acids, the purple denotes the alkalinity of amino acids, the cyan denotes the polar amino acids, and the grey points of ligand atoms denote the solvent accessibility. (For interpretation of the references to color in this figure legend, the reader is referred to the web version of this article.)

RXRα. The phenyl ring-A of **WA15** π stacks (distance: 3.76 Å) with the PHE318 benzene ring. Besides, the hydrophobic interactions of the Ad moiety with hydrophobic residues in RXRα-LBD are observed, suggesting that the hydrophobic nature of the Ad moiety facilitates the positioning and stabilization of **WA15** in RXRα-LBP. Moreover, we used the MM-GBSA module integrated into Schrödinger soft to calculate the $\triangle G_{bind}$ values of the compoud/RXRα complexes. Compared with the native ligand LG100754 ($\triangle G_{bind} = -98.498$ kcal/mol), **WA15** ($\triangle G_{bind} = -76.123$ kcal/mol) showed a relatively lower binding affinity to RXRα, but higher than MX781 ($\triangle G_{bind} = -72.381$ kcal/mol), WA11 ($\triangle G_{bind} = -51.435$ kcal/mol), and WA 24 ($\triangle G_{bind} = -57.468$ kcal/mol). The results of the binding energy are consistent with the docking scores. The predicted binding models of MX781/RXRα, **WA11**/RXRα and **WA24**/RXRα complexes can be found in Figs. S2–S4 in Supplementary Material. The strong interactions in **WA15**/RXRα complex are found to become weak or disappear in **WA11**/RXRα and **WA24**/RXRα complexes, which helps explain the strong binding affinity and anticancer activity of **WA15** compared with those of **WA11** and **WA24**.

2.2.4. *The pro-apoptotic effect of **WA15** in cancer cells*

Apoptosis is the most widely recognized form of programmed cell death and the induction of apoptosis is a common way for cancer therapy. Herein, to examine whether the antitumor activity **WA15** was associated with apoptosis, we further evaluated the apoptotic effect of **WA15** in NCI-H292 cancer cells by flow cytometry. The assay was performed at six different doses (5, 7.5, 10, 15, and 20 μM) for 12 h, the results of which were summarized in Fig. 5. It was found that **WA15** displayed a clear dose-dependent apoptotic effect in NCI-H292 cells, with the percentages of apoptosis cells increasing from 15.65 up to 68.89%. Moreover, we found that **WA15** mainly increased late apoptotic cells in a dose-dependent manner in NCI-H292 cells, with the percentages of late apoptosis cells increasing from 13.77 at 5 μM up to 68.60% at 20 μM.

Next, we evaluated the apoptotic effect of **WA15** at the protein level in cancer cells. The expression levels of RXRα and cleaved PARP (a specific apoptosis-associated protein) were examined by immunoblotting in several cancer cell lines after treatment with or without **WA15** at 10 μM for 12 h. As shown in Fig. 6A and B, **WA15** decreased RXRα protein level and increased PARP cleavage in HepG2, A549, HeLa, and H292 cells. It was also found that **WA15** downregulated RXRα and induced PARP cleavage in a time- and dose- dependent manner in H292 cells (Fig. 6B). Moreover, the RXRα decrease induced by **WA15** was completely blocked by co-treatment of a proteasome inhibitor (MG132), suggesting that **WA15** might lead to RXRα degradation in a proteasome-dependent mechanism (Fig. 6C). To further verify whether **WA15** induced RXRα-dependent apoptosis, the RXRα knockdown (siRXRα) H292 cells were employed to evaluate for the effect on the role of **WA15** in apoptosis induction. Fig. 6D illustrated that transfection of RXRα siRNA reduced the levels of RXRα, while significantly enhanced **WA15**-induced PARP cleavage. Taken together, the RXRα antagonist **WA15** is a member of the fairly heterogeneous group of atypical AdArs [38], the apoptogenic and cell growth inhibitory activities of **WA15** do not result from its inhibition on RXRα transactivation, but RXRα degradation plays a crucial role in **WA15**-induced apoptosis.

2.2.5. ***WA15** inhibits TNFα activation of the NF-κB signaling pathway*

The TNFα/NF-κB pathway plays an important role in the regulation of inflammation, cell proliferation, differentiation, and apoptosis through activation of IκB kinase, and subsequent IκB protein degradation and NF-κB nuclear translocation. Numerous studies have reported that RXRα can mediate the TNFα/NF-κB signaling activation and some RXRα ligands can inhibit the TNFα-induced NF-κB pathway [27]. Besides, it was demonstrated that AdArs reported previously could inhibit IκB Kinase [38,39]. So we speculated if compound **WA15** could regulate the TNFα/NF-κB pathway. As shown in Fig. 7, **WA15** could dose-dependently inhibit the TNFα-induced IκBα degradation and IKKα/β phosphorylation, suggesting that the anticancer activity of **WA15** might be related to the inhibition of IKK/NF-κB signaling.

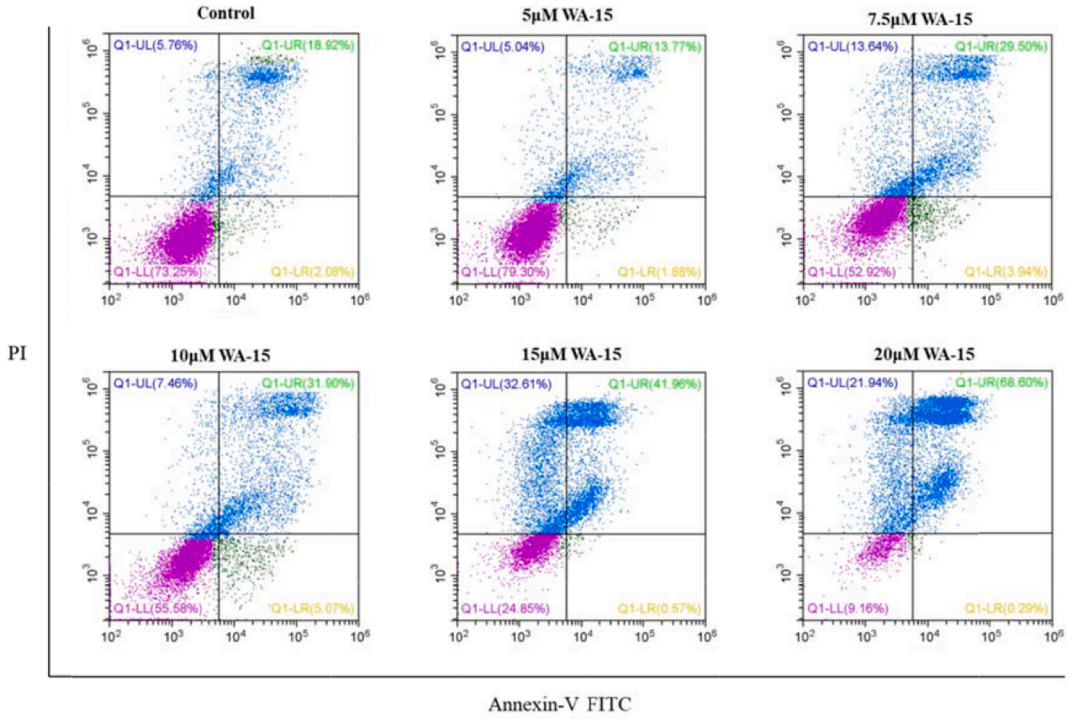

Fig. 5. The **WA15**-induced apoptosis in H292 cells using flow cytometry analysis. H292 cells were treated with **WA15** at the indicated concentrations for 12 h and analyzed by annexin V/PI staining. The cells undergoing apoptosis were defined as two kinds of apoptosis (early apoptosis annexin V-positive cells and late apoptosis annexin V-positive and PI-positive cells).

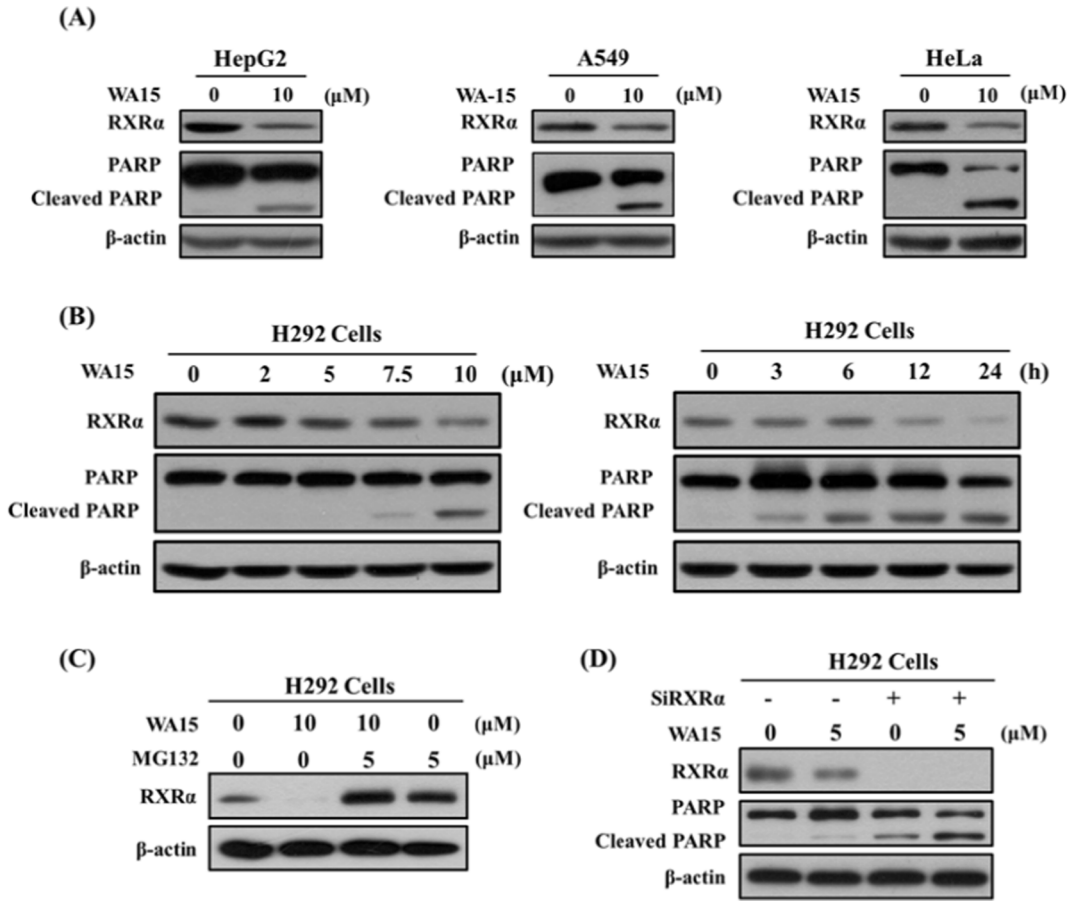

Fig. 6. **WA15**-induced RXRα degradation and PARP cleavage in cancer cells. (A) HepG2, A549, and Hela cells were treated with **WA15** for 12 h and cell lysates prepared were analyzed by Western blotting. (B) H292 cells were time- and dose- dependently treated with **WA15** for the indicated time and cell lysates prepared were analyzed by Western blotting for RXRα degradation and PARP cleavage. (C) Confirmation of proteasome-based mechanism in driving RXRα degradation upon **WA15** treatment. H292 cells were treated overnight with **WA15** (10 μM) alone, MG132 (5 mM) alone, or a combination of **WA15** with MG132; lysates were collected and analyzed by Western blotting for RXRα. (D) Suppression of RXRα expression enhanced the induction of apoptosis by **WA15**. H292 and RXRα-/- H292 cells were treated with **WA15** for 12 h and cell lysates prepared were analyzed by Western blotting for PARP cleavage.

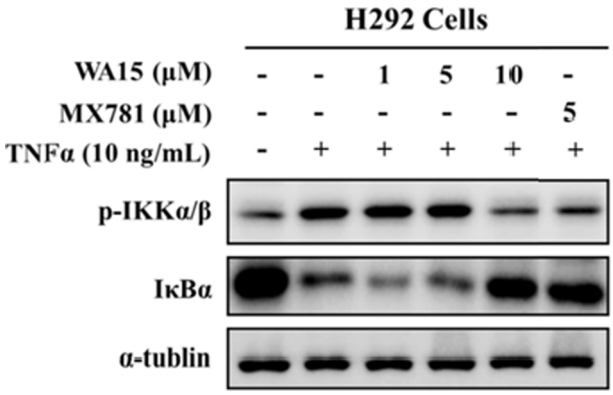

Fig. 7. The effect of **WA15** on TNFα-induced IκBα degradation and IKKα/β phosphorylation. H292 cells pretreated with **WA15** for 1 h were exposed to TNFα (10 ng/mL) for 30 min, and IKKα/β phosphorylation and IκBα expression were analyzed by immunoblotting.

3. Conclusion

In summary, a new class of chalcone AdArs was synthesized as anticancer agents and RXRα modulators. Among synthesized compounds, **WA15** was identified as the most potent anticancer agent and displayed over 5-fold higher selectivity in killing cancer over normal cells. To our surprise, **WA15** does not belong to RAR antagonists like its parent compound MX781. On the contrary, **WA15** could selectively bind to RXRα-LBD and effectively inhibit the transcriptional activity of RXRα. We also confirmed that **WA15** promoted the apoptosis of cancer cells in an RXRα-independent way, which is similar to other AdArs reported previously. Besides, **WA15** induced the proteasome-dependent degradation of RXRα and suppression of RXRα expression using siRNA technology enhanced the **WA15**-induced apoptosis. Further experiments indicated that the anticancer activity of **WA15** might be related to the inhibition of IKK/NF-κB signaling. Taken together, **WA15** may be served as a good starting point to design and synthesis new low-toxicity anticancer agents and RXRα degraders.

4. Experimental section

4.1. Chemistry

Benzaldehydes **1a-b** and substituted acetophenones **6a-h** were commercially available, except for **6e** which was synthesized. The other reagents were purchased and used without further purification, unless otherwise indicated. Reactions were magnetically stirred and monitored by thin-layer chromatography (TLC) on Merck silica gel 60 F254 by fluorescence. All of the final compounds were purified by flash column chromatography on silica gel (Merck 230–400 mesh). ^{1}H NMR and ^{13}C NMR spectra were obtained using a Bruker AV2 600 Ultra shield spectrometer at 600 and 150 MHz, respectively. Chemical shifts were given

in parts per million (ppm) relative to tetramethylsilane (TMS) as an internal standard and coupling constants (*J*) are given in Hertz (Hz). Splitting patterns are designated as follows: singlet (s), doublet (d), doublet of doublet (dd), triplet (t), multiplet (m), and broad signal (br. s.). High-resolution mass spectra (HRMS) were determined on a Q Exactive LC-MS/MS instrument equipped with electrospray ionization (ESI) source (Thermo Fisher Scientific Inc., Waltham, MA, USA). The electrospray ionization mass spectrometry was carried out with an Agilent 1100 SL instrument. Melting points were determined with a micro-melting point spectrometer (SGW X-4) and were uncorrected.

4.1.1. The synthesis of 3-(Adamant-1-yl)-4-hydroxybenzaldehyde (2a)

To a solution of 4-hydroxybenzaldehyde **1a** (1.22 g, 10 mmol) in CH_2Cl_2 (40 mL) was added adamant-1-ol (1.69 g, 11.1 mmol) and H_2SO_4 (0.65 mL, 12 mmol). The reaction mixture was stirred at 50 °C for 16 h. After addition of a saturated aqueous $NaHCO_3$ solution until neutral pH was reached, the mixture was extracted with ethyl acetate (50 mL × 3). The combined organic layer was dried over anhydrous Na_2SO_4 and evaporated. The crude was purified by chromatography (silica gel, hexane/EtOAc = 20:1) to afford **2a**. White solid, yield 51.4%. ^{1}H NMR (600 MHz, DMSO-d_6): δ 9.78 (s, 1H), 7.66 (d, J = 2.1 Hz, 1H), 7.60 (dd, J = 2.1, 8.3 Hz, 1H), 6.94 (d, J = 8.3 Hz, 1H), 2.04–2.08 (m, 9H), 1.72–1.76 (m, 6H). ^{13}C NMR (150 MHz, DMSO-d_6): δ 191.6, 160.6, 137.2, 129.9, 129.7, 128.2, 117.3, 40.3 (3C), 37.0 (3C), 36.9, 28.9 (3C). ESI-MS (–): m/z 255.0 $[M-H]^-$.

4.1.2. The synthesis of 5-(Adamant-1-yl)-2,4-dihydroxybenzaldehyde (2b)

Following the same procedure for **2a**, 2,4-dihydroxybenzaldehyde **1b** (1.38 g, 10 mmol) and adamant-1-ol (1.69 g, 11.1 mmol) were afforded to give **2b.** White solid, yield: 76.8%. ^{1}H NMR (600 MHz, $CDCl_3$): δ 11.24 (s, 1H), 9.73 (s, 1H), 7.36 (s, 1H), 6.26 (s, 1H), 2.08–2.11 (m, 9H), 1.78–1.83 (m, 6H). ^{13}C NMR (150 MHz, $CDCl_3$): δ 194.9, 162.7, 162.0, 133.1, 130.0, 115.1, 104.3, 40.7 (3C), 36.9 (3C), 36.2, 28.9 (3C); ESI-MS (–): m/z 270.2 $[M-H]^-$.

4.1.3. The synthesis of 3-(Adamant-1-yl)-4-(methoxymethoxy)-benzaldehyde (3a)

A mixture of 3-(adamant-1-yl)-4-hydroxybenzaldehyde **2a** (1.04 g, 4.06 mmol), chloromethyl methyl ether (MOMCl) (1.0 mL, 8.12 mmol) and anhydrous potassium carbonate (1.68 g, 12.18 mmol) in 100 mL of acetone was stirred at 60 °C for 6 h. The resulting mixture was filtered off and the filtrate was concentrated in vacuum to give an oil, which was purified by silica gel chromatography eluted with hexane/EtOAc = 30:1 to give **3a.** White solid, yield 88.1%. ^{1}H NMR (600 MHz, $CDCl_3$): δ 9.91 (s, 1H), 7.83 (d, J = 2.0 Hz, 1H), 7.72 (dd, J = 2.0, 8.3 Hz, 1H), 7.22 (d, J = 8.3 Hz, 1H), 5.33 (s, 2H), 3.55 (s, 3H), 2.11–2.16 (m, 9H), 1.80–1.82 (m, 6H). ^{13}C NMR (150 MHz, $CDCl_3$): δ 191.5, 161.4, 139.3, 130.3, 130.0, 128.6, 114.3, 94.0, 56.6, 40.5 (3C), 37.3 (3C), 37.0, 28.9 (3C). ESI-MS (+): m/z 301.0 $[M + H]^+$.

4.1.4. 3-(Adamantan-1-yl)-4-(benzyloxy)benzaldehyde (3b)

Following the same procedure for **3a**, the reaction of **2a** (1.04 g, 4.06 mmol) and benzyl bromide (0.76 g, 4.47 mmol) afforded to **3b**. White solid, yield: 80.3%. ^{1}H NMR (600 MHz, $CDCl_3$): δ 9.91 (s, 1H), 7.85 (d, J = 2.1 Hz, 1H), 7.74 (dd, J = 2.1, 8.3 Hz, 1H), 7.53–7.37 (m, 5H), 7.08 (d, J = 8.3 Hz, 1H), 5.23 (s, 2H), 2.07–2.19 (m, 9H), 1.72–1.79 (m, 6H). ^{13}C NMR (150 MHz, $CDCl_3$): δ 191.4, 162.9, 139.3, 136.2, 130.2, 129.8, 128.7 (2C), 128.6, 127.4, 127.3 (2C), 112.4, 70.5, 40.3 (3C), 37.3 (3C), 37.0, 28.9 (3C). ESI-MS (m/z): 347.1, $[M + H]^+$.

4.1.5. The synthesis of 5-(Adamant-1-yl)-2,4-bis(methoxymethoxy)-benzaldehyde (3c)

Following the same procedure for **3a**, the reaction of **2b** (1.36 g, 5 mmol) and MOMCl (2.1 mL, 17.5 mmol) afforded to **3c**. White solid, yield: 82.3%. ^{1}H NMR (600 MHz, $CDCl_3$): δ 10.34 (s, 1H), 7.74 (s, 1H), 6.90 (s, 1H), 5.29 (d, J = 8.8 Hz, 4H), 3.53 (d, J = 5.0 Hz, 6H), 2.07–2.10 (m, 9H), 1.75–1.78 (m, 6H). ^{13}C NMR (150 MHz, $CDCl_3$): δ 188.5, 162.5, 159.7, 132.9, 126.8, 119.1, 101.0, 94.8, 94.1, 56.7, 56.5, 40.7 (3C), 37.0 (3C), 36.7, 29.0 (3C). ESI-MS (+): m/z 361.0 $[M + H]^+$.

4.1.6. The synthesis of Methyl-4-acetoxybenzoate (5)

To a solution of methyl 4-hydroxybenzoate **4** (10.0 mmol) in acetic acid anhydride (5 mL) was added 5 drops of concentrated sulfuric acid and the mixture was stirred at room temperature for 2 h. After the reaction was completed, the mixture was poured into ice water, and the solid was filtered, washed with Na_2CO_3 and water twice. After natural drying to get methyl 4-hydroxybenzoate as a white solid (92.7%), which was used without any further purification.

4.1.7. The synthesis of 3-acetyl-4-hydroxybenzoic acid (6e)

In a 100 mL three-necked flask equipped with water condenser and gas absorber, methyl 4-acetoxybenzoate **5** (1.36 g, 7.0 mmol) and anhydrous $AlCl_3$ (2.77 g, 21 mmol) were mixed and heated at 160 °C (oil bath temperature) for 5 h. After cooling in an ice bath, the reaction mixture was treated with 20 mL of 2 M HCl. The acidified reaction mixture was extracted with ethyl acetate (3 × 50 mL). The combined organic layer was dried over anhydrous Na_2SO_4, filtered, and concentrated. The crude was recrystallized with ethanol to give 3-acetyl-4-hydroxybenzoic acid **6e.** White solid, yield 53.1%. ^{1}H NMR (600 MHz, DMSO-d_6): δ 12.24 (s, 1H), 8.37 (d, J = 2.1 Hz, 1H), 8.03 (dd, J = 2.1, 8.8 Hz, 1H), 7.04 (d, J = 8.8 Hz, 1H), 2.67 (s, 3H). ^{13}C NMR (150 MHz, DMSO-d_6): δ 203.8, 166.8, 164.2, 136.8, 133.4, 122.1, 121.2, 118.3, 28.7. ESI-MS: m/z 179.0 $[M-H]^-$.

4.1.8. General method for the synthesis of chalcone derivatives WA1-WA18.

To a solution of one acetophenone (**6a-6h**, 1 mmol) and one benzaldehyde derivative (**3a-3c**, 1.1 mmol) in MeOH (8 mL) was added 40% aqueous sodium hydroxide (2 mL). The reaction mixture was heated at 70 °C for 4–16 h. The progress of the reaction was monitored by TLC. After completion, the reaction mixture was cooled to 0 °C on an ice bath and acidified with 1 N HCl until pH = 5–6 was reached. The crude product was extracted with CH_2Cl_2 (50 mL × 3) and purified over silica gel column chromatography to give the corresponding chalcone AdAr (**WA1-WA18**).

*(E)-3-(3-(adamantan-1-yl)-4-(methoxymethoxy)phenyl)-1-(2-hydroxyphenyl)prop-2-en-1-one (**WA1**).* 1-(2-hydroxyphenyl)ethanone **6a** was reacted with 3-(adamant-1-yl)-4-(methoxymethoxy)-benzaldehyde **3a** to give **WA1**. Yellow solid; yield 50.6%; Mp: 159–161 °C. ^{1}H NMR (600 MHz, $CDCl_3$): δ 12.98 (s, 1H), 7.94 (dd, J = 8.3, 2.0 Hz, 1H), 7.92 (d, J = 15.3 Hz, 1H), 7.50–7.55 (m, 2H), 7.44–7.50 (m, 2H), 7.12 (d, J = 8.3 Hz, 1H), 7.02 (d, J = 8.3 Hz, 1H), 6.91–6.96 (m, 1H), 5.27 (s, 2H), 3.52 (s, 3H), 2.08–2.17 (m, 9H), 1.78–1.82 (m, 6H). ^{13}C NMR (150 MHz, $CDCl_3$): δ 193.7, 163.6, 158.9, 146.2, 139.2, 136.1, 129.6, 128.0, 127.9, 127.9, 120.2, 118.7, 118.6, 117.5, 114.7, 94.1, 56.5, 40.6 (3C), 37.2, 37.1 (3C), 29.0 (3C). ESI-HRMS (–): m/z $[M-H]^-$ calculated for $C_{27}H_{29}O_4^-$ 417.2071, found 417.2073.

*(E)-3-(3-(adamantan-1-yl)-4-(methoxymethoxy)phenyl)-1-(2-hydroxy-5-methylphenyl)prop-2-en-1-one (**WA2**).* The reaction of 1-(2-hydroxy-5-methylphenyl)ethanone **6b** and **3a** gave **WA2**. Yellow solid; yield 57.2%; Mp: 123–125 °C. ^{1}H NMR (600 MHz, $CDCl_3$): δ 12.79 (s, 1H), 7.89 (d, J = 15.3 Hz, 1H), 7.68 (d, J = 2.0 Hz, 1H), 7.52–7.53 (m, 2H), 7.48–7.51 (m, 1H), 7.28 (dd, J = 2.0, 8.3 Hz, 1H), 7.13 (d, J = 8.3 Hz, 1H), 6.92 (d, J = 8.3 Hz, 1H), 5.27 (s, 2H), 3.52 (s, 3H), 2.35 (s, 3H), 2.11–2.15 (m, 9H), 1.78–1.82 (m, 6H). ^{13}C NMR (150 MHz, $CDCl_3$): δ 193.5, 161.3, 158.6, 145.9, 139.0, 137.0, 129.1, 128.1, 127.8, 127.6, 127.4, 119.7, 118.1, 117.5, 114.6, 94.1, 56.5, 40.6 (3C), 37.2, 37.1 (3C), 29.0 (3C), 20.7. ESI-HRMS (–): m/z $[M-H]^-$ calculated for $C_{28}H_{31}O_4^-$ 431.2228, found 431.2230.

*(E)-3-(3-(adamantan-1-yl)-4-(methoxymethoxy)phenyl)-1-(5-chloro-2-hydroxyphenyl)prop-2-en-1-one (**WA3**).* The reaction of 1-(5-chloro-2-hydroxyphenyl)ethanone **6c** and **3a** gave **WA3**. Yellow solid; yield

53.1%; Mp: 122–123 °C. ^{1}H NMR (600 MHz, $CDCl_3$): δ 12.90 (s, 1H), 7.93 (d, J = 15.3 Hz, 1H), 7.87 (d, J = 1.8 Hz, 1H), 7.49–7.56 (m, 2H), 7.38–7.45 (m, 2H), 7.14 (d, J = 8.3 Hz, 1H), 6.97 (d, J = 8.3 Hz, 1H), 5.30 (s, 2H), 3.55 (s, 3H), 2.09–2.18 (m, 9H), 1.78–1.83 (m, 6H). ^{13}C NMR (150 MHz, $CDCl_3$): δ 191.8, 161.0, 158.1, 146.3, 138.3, 134.8, 127.7, 127.4, 127.0, 126.6, 122.3, 119.8, 119.1, 115.8, 113.8, 93.0, 55.5, 39.5 (3C), 36.3, 36.0 (3C), 28.0 (3C). ESI-HRMS (–): *m/z* $[M-H]^-$ calculated for $C_{27}H_{28}ClO_4^-$ 451.1682 and 453.1652, found 451.1679 and 453.1655.

*(E)-3-(3-(adamantan-1-yl)-4-(methoxymethoxy)phenyl)-1-(2-hydroxy-5-methoxyphenyl)prop-2-en-1-one (**WA4**)*. The reaction of 1-(2-hydroxy-5-methoxyphenyl)ethanone **6d** and **3a** gave **WA4**. Yellow solid; yield 50.4%; Mp: 110–112 °C. ^{1}H NMR (600 MHz, $CDCl_3$): δ 12.49 (s, 1H), 7.90 (d, J = 15.3 Hz, 1H), 7.53 (d, J = 2.3 Hz, 1H), 7.49 (dd, J = 2.3, 8.5 Hz, 1H), 7.45 (d, J = 15.3 Hz, 1H), 7.38 (d, J = 3.0 Hz, 1H), 7.13 (d, J = 8.5 Hz, 1H), 7.12 (dd, J = 3.0, 9.0 Hz, 1H), 6.96 (d, J = 9.0 Hz, 1H), 5.28 (s, 2H), 3.83 (s, 3H), 3.53 (s, 3H), 2.08–2.16 (m, 9H), 1.78–1.82 (m, 6H). ^{13}C NMR (150 MHz, $CDCl_3$): δ 193.4, 158.9, 157.8, 151.6, 146.4, 139.2, 128.2, 127.8, 127.7, 123.2, 119.9, 119.2, 117.6, 114.7, 113.4, 94.1, 56.5, 56.2, 40.5 (3C), 37.2, 37.0 (3C), 29.0 (3C). ESI-HRMS (–): *m/z* $[M-H]^-$ calculated for $C_{28}H_{31}O_5^-$ 447.2177, found 447.2177.

*(E)-3-[(3-adamantan-1-yl)-4-(methoxymethoxy)phenyl)acryloyl]-4-hydroxybenzoic acid (**WA5**)*. The reaction of 3-acetyl-4-hydroxybenzoic acid **6e** and **3a** gave **WA5**. Red solid; yield 40.5%; Mp: 202–205 °C. ^{1}H NMR (600 MHz, DMSO-d_6): δ 8.57 (d, J = 2.2 Hz, 1H), 8.10 (d, J = 2.2, 8.6 Hz, 1H), 7.85 (d, J = 15.3 Hz, 1H), 7.80–7.82 (m, 2H), 7.64 (d, J = 2.2 Hz, 1H), 7.15 (d, J = 8.6 Hz, 1H), 7.13 (d, J = 8.6 Hz, 1H), 5.38 (s, 2H), 3.50 (s, 3H), 2.10–2.16 (m, 9H), 1.79–1.83 (m, 6H). ^{13}C NMR (150 MHz, DMSO-d_6): δ 193.2, 167.0, 164.4, 158.6, 146.1, 138.7, 136.4, 132.7, 128.8, 128.7, 127.8, 122.5, 122.2, 120.8, 118.3. 115.1, 94.2, 56.7, 40.4 (3C), 37.1, 36.9 (3C), 28.8 (3C). ESI-HRMS (–): *m/z* $[M-H]^-$ calculated for $C_{28}H_{29}O_6^-$ 461.1970, found 461.1974.

*(E)-3-(3-adamantan-1-yl)-4-(benzyloxy)phenyl)-1-(2-hydroxyphenyl) prop-2-en-1-one (**WA6**)*. The reaction of **6a** and 3-(adamant-1-yl)-4-(benzyloxy)-benzaldehyde (**3b**) gave **WA6**. Red solid; yield 57.8%; Mp: 150–152 °C. ^{1}H NMR (600 MHz, $CDCl_3$): δ 12.91 (s, 1H), 7.85–7.88 (m, 2H), 7.51 (d, J = 2.2 Hz, 1H), 7.46 (d, J = 15.3 Hz, 1H), 7.42–7.43 (m, 4H), 7.35 (t, J = 7.5 Hz, 2H), 7.29 (d, J = 7.5 Hz, 1H), 6.95 (dd, J = 1.1, 8.4 Hz, 1H), 6.91 (d, J = 8.4 Hz, 1H), 6.88 (td, J = 7.5, 1.1 Hz, 1H), 5.11 (s, 2H), 2.09–2.12 (m, 6H), 1.99–2.02 (m, 3H), 1.66–1.70 (m, 6H). ^{13}C NMR (150 MHz, $CDCl_3$): δ 193.7, 163.6, 160.4, 146.3, 139.1, 136.6, 136.0, 129.5, 128.6, 128.2, 127.8, 127.3, 126.7, 124.4, 121.9, 118.7, 117.2, 112.9, 70.3, 40.5 (3C), 37.2, 37.1 (3C), 29.0 (3C). ESI-HRMS (–): *m/z* $[M-H]^-$ calculated for $C_{32}H_{31}O_3^-$, 463.2279, found 463.2284.

*(E)-3-(3-adamantan-1-yl)-4-(benzyloxy)phenyl)-1-(2-hydroxy-5-methylphenyl)prop-2-en-1-one (**WA7**)*. The reaction of **6b** and **3b** gave **WA7**. Red solid; yield 42.8%; Mp: 101–103 °C. ^{1}H NMR (600 MHz, $CDCl_3$): δ 12.81 (s, 1H), 7.93 (d, J = 15.3 Hz, 1H), 7.68 (s, 1H), 7.48–7.55 (m, 5H), 7.39–7.44 (m, 2H), 7.37 (d, J = 8.0 Hz, 1H), 7.30 (d, J = 8.0 Hz, 1H), 6.98 (d, J = 8.5 Hz, 1H), 6.94 (d, J = 8.5 Hz, 1H), 5.17 (s, 2H), 2.36 (s, 3H), 2.07–2.17 (m, 9H), 1.72–1.76 (m, 6H). ^{13}C NMR (150 MHz, $CDCl_3$): δ 192.6, 160.5, 159.3, 145.1, 138.2, 136.1, 135.6, 128.2, 127.6 (2C), 127.1, 127.0, 126.8, 126.7, 126.3 (2C), 126.2, 118.8, 117.3, 116.4, 111.9, 69.3, 39.4 (3C), 36.2, 36.0 (3C), 28.0 (3C), 19.7. ESI-HRMS (–): *m/z* $[M-H]^-$ calculated for $C_{33}H_{33}O_3^-$ 477.2435, found 477.2439.

*(E)-3-(3-adamantan-1-yl)-4-(benzyloxy)phenyl)-1-(5-chloro-2-hydroxyphenyl)prop-2-en-1-one (**WA8**)*. The reaction of **6c** and **3b** gave **WA8**. Yellow solid; yield 51.8%; Mp: 161–163 °C. ^{1}H NMR (600 MHz, CDCl3): δ 12.90 (s, 1H), 7.94 (d, J = 15.3 Hz, 1H), 7.86 (d, J = 2.5 Hz, 1H), 7.56 (d, J = 2.5 Hz, 1H), 7.52 (dd, J = 2.0, 8.5 Hz, 1H), 7.46–4.50 (m, 2H), 7.38–7.43 (m, 4H), 7.34–7.37 (m, 1H), 6.98 (d, J = 3.5 Hz, 1H), 6.96 (d, J = 3.5 Hz, 1H), 5.18 (s, 2H), 2.08–2.17 (m, 9H), 1.71–1.78 (m, 6H). ^{13}C NMR (150 MHz, $CDCl_3$): δ 191.7, 161.0, 159.7, 146.4, 138.3, 135.5, 134.8, 127.7, 127.6 (2C), 127.3, 127.2, 127.0, 126.3 (2C), 125.9, 122.3, 119.8, 119.1, 115.5, 111.9, 69.4, 39.4 (3C), 36.2, 36.0 (3C), 28.0 (3C). ESI-HRMS (–): *m/z* $[M-H]^-$ calculated for $C_{32}H_{30}ClO_3^-$ 497.1889 and 498.1923, found 497.1878 and 498.1917.

*(E)-3-(3-adamantan-1-yl)-4-(benzyloxy)phenyl)-1-(2-hydroxy-5-methoxyphenyl)prop-2-en-1-one (**WA9**)*. The reaction of **6d** and **3b** gave **WA9**. Red solid; yield 61.8%; Mp: 113–116 °C. ^{1}H NMR (600 MHz, $CDCl_3$): δ 12.54 (s, 1H), 7.92 (d, J = 15.3 Hz, 1H), 7.53 (s, 1H), 7.45–7.48 (m, 3H), 7.33–7.41 (m, 5H), 7.12 (dd, J = 3.0, 9.0 Hz, 1H), 6.93–6.96 (m, 2H), 5.14 (s, 2H), 3.81 (s, 3H), 2.06–2.16 (m, 9H), 1.71–1.77 (m, 6H). ^{13}C NMR (150 MHz, $CDCl_3$): δ 192.3, 159.3, 156.8, 150.6, 145.4, 138.1, 135.6, 127.6 (2C), 127.0, 126.9 (2C), 126.3 (2C), 126.1, 122.0, 118.9, 118.1, 116.2, 112.4, 111.8, 69.3, 55.1, 39.3 (3C), 36.1, 35.9 (3C), 27.9 (3C). ESI-HRMS (–): *m/z* $[M-H]^-$ calculated for $C_{33}H_{33}O_4^-$ 493.2384, found 493.2384.

*3-[(E)-3-(3-(adamantan-1-yl)-4-(benzyloxy)phenyl)acryloyl]-4-hydroxybenzoic acid (**WA10**)*. The reaction of **6e** and **3b** gave **WA10**. Red solid; yield 30.5%; Mp: 180–183 °C. ^{1}H NMR (600 MHz, $CDCl_3$): δ 8.60 (d, J = 2.0 Hz, 1H), 8.06 (dd, J = 2.0, 8.8 Hz, 1H), 7.91 (d, J = 15.3 Hz, 1H), 7.49–7.53 (m, 3H), 7.42–7.43 (m, 2H), 7.35 (t, J = 7.3 Hz, 2H), 7.29 (m, 1H), 6.97 (d, J = 8.4 Hz, 1H), 6.93 (d, J = 8.4 Hz, 1H), 5.13 (s, 2H), 2.00–2.11 (m, 9H), 1.65–1.69 (m, 6H). ^{13}C NMR (150 MHz, $CDCl_3$): δ 192.5, 166.3, 165.3, 159.6, 146.6, 138.3, 135.7, 135.5, 131.1, 127.7, 127.6, 127.1, 127.0, 126.3, 125.9, 119.7, 118.6, 117.7, 115.5, 111.9, 69.4, 39.3 (2C), 36.2, 35.9 (2C), 27.9 (2C). ESI-HRMS (–): *m/z* $[M-H]^-$ calculated for $C_{33}H_{31}O_5^-$ 507.2177, found 507.2168.

*(E)-3-(5-(adamantan-1-yl)-2,4-bis(methoxymethoxy)phenyl)-1-(2-hydroxyphenyl)prop-2-en-1-one (**WA11**)*. The reaction of 6a and 5-(adamantan-1-yl)-2,4-bis(methoxymethoxy)-benzaldehyde (3c) gave **WA11**. Yellow solid; yield 60.5%; Mp: 108–110 °C. ^{1}H NMR (600 MHz, $CDCl_3$): δ 13.08 (s, 1H), 8.24 (d, J = 15.3 Hz, 1H), 7.93 (dd, J = 8.4, 1.5 Hz, 1H), 7.66 (d, J = 15.3 Hz, 1H), 7.52 (s, 1H), 7.46–7.52 (m, 1H), 7.26 (s, 1H), 7.02 (dd, J = 8.4, 1.5 Hz, 1H), 6.92–6.97 (m, 2H), 5.28 (s, 2H), 5.27 (s, 2H), 3.54 (s, 3H), 3.53 (s, 3H), 2.08–2.14 (m, 9H), 1.78–1.81 (m, 6H). ^{13}C NMR (150 MHz, $CDCl_3$): δ 193.2, 162.6, 158.8, 155.4, 140.6, 134.9, 131.8, 128.6, 126.6, 119.4, 117.6, 117.5, 117.0, 116.1, 100.8, 93.9, 93.3, 55.6, 55.5, 39.8 (3C), 36.0 (3C), 35.7, 28.0 (3C). ESI-HRMS (–): *m/z* calculated for $C_{29}H_{33}O_6^-$ 477.2283, found 477.2282.

*(E)-3-(5-(adamantan-1-yl)-2,4-bis(methoxymethoxy)pheny)-1-(2-hydroxy-5-methylphenyl)prop-2-en-1-one (**WA12**)*. The reaction of **6b** and **3c** gave **WA12**. Yellow solid; yield 65.4%; Mp: 114–116 °C. ^{1}H NMR (600 MHz, DMSO-d_6): δ 12.88 (s, 1H), 8.21 (d, J = 15.6 Hz, 1H), 7.69 (d, J = 2.0 Hz, 1H), 7.66 (d, J = 15.6 Hz, 1H), 7.51 (s, 1H), 7.28 (dd, J = 2.0, 8.4 Hz, 1H), 6.93 (s, 1H), 6.92 (d, J = 8.4 Hz, 1H), 5.27 (s, 2H), 5.26 (s, 2H), 3.53 (s, 6H), 2.35 (s, 3H), 2.08–2.15 (m, 9H), 1.78–1.81 (m, 6H). ^{13}C NMR (150 MHz, $CDCl_3$): δ 193.2, 160.4, 158.7, 155.3, 140.4, 135.9, 131.7, 128.3, 126.7, 126.6, 119.0, 117.2, 116.2, 100.8, 93.9, 93.2, 55.6, 55.5, 39.8 (3C), 36.0 (3C), 35.7, 28.0 (3C), 19.7. ESI-HRMS (–): *m/z* $[M-H]^-$ calculated for $C_{30}H_{35}O_6^-$ 491.2439, found 491.2430.

*(E)-3-(5-(adamantan-1-yl)-2,4-bis(methoxymethoxy)phenyl)-1-(5-chloro-2-hydroxyphenyl)prop-2-en-1-one (**WA13**)*. The reaction of **6c** and **3c** gave **WA13**. Yellow solid; yield 63.4%; Mp: 140–143 °C. ^{1}H NMR (600 MHz, $CDCl_3$): δ 13.00 (s, 1H), 8.24 (d, J = 15.6 Hz, 1H), 7.87 (d, J = 2.5 Hz, 1H), 7.57 (d, J = 15.6 Hz, 1H), 7.50 (s, 1H), 7.41 (dd, J = 2.5, 9.0 Hz, 1H), 6.97 (d, J = 9.0 Hz, 1H), 6.94 (s, 1H), 5.29 (s, 2H), 5.27 (s, 2H), 3.55 (s, 3H), 3.54 (s, 3H), 2.10–2.13 (m, 9H), 1.78–1.82 (m, 6H). ^{13}C NMR (150 MHz, $CDCl_3$): δ 192.3, 161.0, 159.1, 155.6, 141.8, 134.6, 131.9, 127.8, 127.0, 122.2, 120.0, 119.1, 116.3, 115.8, 100.7, 93.9, 93.2, 55.6, 55.6, 39.8 (3C), 36.0 (3C), 35.7, 28.0 (3C). ESI-HRMS (–): *m/z* $[M-H]^-$ calculated for $C_{29}H_{32}ClO_6^-$ 511.1893 and 513.1863, found 511.1880 and 513.1876.

*(E)-3-(5-(adamantan-1-yl)-2,4-bis(methoxymethoxy)phenyl)-1-(2-hydroxy-5-methoxyphenyl)prop-2-en-1-one (**WA14**)*. The reaction of **6d** and **3c** gave **WA14**. Red solid; yield 53.2%; Mp: 114–116 °C. ^{1}H NMR (600 MHz, $CDCl_3$): δ 12.59 (s, 1H), 8.21 (d, J = 15.6 Hz, 1H), 7.63 (d, J = 15.6 Hz, 1H), 7.50 (s, 1H), 7.40 (d, J = 3.0 Hz, 1H), 7.11 (dd, J = 3.0, 9.0 Hz, 1H), 6.96 (d, J = 9.0 Hz, 1H), 6.94 (s, 1H), 5.28 (s, 2H), 5.27 (s, 2H), 3.83 (s, 3H), 3.53 (s, 3H), 3.53 (s, 3H), 2.07–2.14 (m, 9H),

1.78–1.81 (m, 6H). ^{13}C NMR (150 MHz, $CDCl_3$): δ 192.9, 158.8, 156.8, 155.4, 150.5, 140.8, 131.8, 126.9, 121.9, 119.0, 118.1, 117.2, 116.1, 112.4, 100.7, 93.9, 93.2, 55.6, 55.5, 55.0, 39.8 (3C), 36.0 (3C), 35.7, 28.0 (3C). ESI-HRMS (–): *m/z* $[M-H]^-$ calculated for $C_{30}H_{35}O_7^-$ 507.2388, found 507.2382.

*(E)-3-(3-(5-(adamantan-1-yl)-2,4-bis(methoxymethoxy)phenyl) acryloyl)-4-hydroxybenzoic acid (**WA15**)*. The reaction of **6e** and **3c** gave **WA15**. Yellow solid; yield 30.5%; Mp: 113–115 °C. ^{1}H NMR (600 MHz, $CDCl_3$): δ 8.48 (d, *J* = 2.0 Hz, 1H), 8.03–8.07 (m, 2H), 7.81 (d, *J* = 15.6 Hz, 1H), 7.57 (s, 1H), 7.08 (d, *J* = 8.6 Hz, 1H), 6.85 (s, 1H), 5.33 (s, 2H), 5.32 (s, 2H), 3.47 (s, 3H), 3.45 (s, 3H), 2.06–2.09 (m, 9H), 1.73–1.77 (m, 6H). ^{13}C NMR (150 MHz, $CDCl_3$): δ 193.1, 167.0, 164.4, 159.7, 156.4, 140.7, 136.2, 132.6, 132.4, 127.8, 122.6, 122.2, 120.8, 118.3, 116.7, 102.0, 95.2, 94.5, 56.9, 56.6, 40.7 (3C), 37.0 (3C), 36.7, 28.8 (3C). ESI-HRMS (–): *m/z* $[M-H]^-$ calculated for $C_{30}H_{33}O_8^-$ 521.2181, found 521.2168.

*(E)-3-(5-(adamantan-1-yl)-2,4-bis(methoxymethoxy)phenyl)-1-(m-tolyl)prop-2-en-1-one (**WA16**)*. The reaction of **6f** and **3c** gave **WA16**. Yellow solid; yield 60.5%; Mp: 120–122 °C. ^{1}H NMR (600 MHz, $CDCl_3$): δ 8.02 (d, *J* = 15.8 Hz, 1H), 7.74 (s, 1H), 7.72 (d, *J* = 5.7 Hz, 1H), 7.39–7.45 (m, 2H), 7.27–7.31 (m, 2H), 6.85 (s, 1H), 5.17 (s, 2H), 5.16 (s, 2H), 3.45 (s, 3H), 3.43 (s, 3H), 2.36 (s, 3H), 1.96–2.05 (m, 9H), 1.68–1.73 (m, 6H). ^{13}C NMR (150 MHz, $CDCl_3$): δ 191.4, 159.3, 155.9, 140.7, 138.9, 138.2, 133.0, 132.6, 129.0, 128.3, 127.1, 125.6, 120.6, 117.4, 101.8, 94.9, 94.3, 56.6, 56.5, 40.9 (3C), 37.1 (3C), 36.7, 29.1 (3C), 21.4. ESI-HRMS (+): *m/z* $[M + Na]^-$ calculated for $C_{30}H_{36}O_5Na^+$ 499.2455, found 499.2453.

*(E)-3-(5-(adamantan-1-yl)-2,4-bis(methoxymethoxy)phenyl)-1-(p-tolyl)prop-2-en-1-one (**WA17**)*. The reaction of **6g** and **3c** gave **WA17**. Yellow solid; yield 60.5%; Mp: 115–117 °C. ^{1}H NMR (600 MHz, $CDCl_3$): δ 8.03 (d, *J* = 15.8 Hz, 1H), 7.85 (d, *J* = 7.7 Hz, 2H), 7.44 (t, *J* = 7.7 Hz, 2H), 7.22 (d, *J* = 7.5 Hz, 2H), 6.85 (s, 1H), 5.18 (s, 2H), 5.17 (s, 2H), 3.46 (s, 3H), 3.44 (s, 3H), 2.36 (s, 3H), 2.02–2.04 (m, 9H), 1.70–1.72 (m, 6H). ^{13}C NMR (150 MHz, $CDCl_3$): δ 189.7, 158.3, 154.9, 142.0, 139.4, 135.2, 131.6, 128.6, 128.2, 127.6, 126.1, 119.4, 100.9, 93.9, 93.2, 55.5, 55.4, 39.8 (3C), 36.0 (3C), 35.7, 28.0 (3C), 20.6. ESI-HRMS (+): *m/z* $[M + Na]^+$ calculated for $C_{30}H_{36}O_5Na^+$ 499.2455, found 499.2460.

*(E)-3-(5-(adamantan-1-yl)-2,4-bis(methoxymethoxy)phenyl)-1-(3-(trifluoromethyl)phenyl)prop-2-en-1-one (**WA18**)*. The reaction of **6h** and **3c** gave **WA18**. Yellow solid; yield 58.7%; Mp: 131–133 °C. ^{1}H NMR (600 MHz, $CDCl_3$): δ 8.17 (s, 1H), 8.09 (d, *J* = 7.5 Hz, 1H), 8.01–8.07 (m, 1H), 7.73 (d, *J* = 7.5 Hz, 1H), 7.56 (t, *J* = 7.7 Hz, 1H), 7.38–7.47 (m, 1H), 6.86 (s, 1H), 5.19 (s, 2H), 5.18 (s, 2H), 3.46 (s, 3H), 3.44 (s, 3H), 2.05–2.02 (m, 9H), 1.72–1.70 (m, 6H). ^{13}C NMR (150 MHz, $CDCl_3$): δ 189.0, 158.7, 155.2, 141.3, 138.5, 131.8, 130.6, 128.1, 127.6, 127.6, 126.6, 124.3, 121.9, 118.7, 115.9, 100.7, 93.8, 93.2, 55.6, 55.5, 39.8 (3C), 36.0 (3C), 35.7, 28.7 (3C), 28.0. ESI-HRMS (+): *m/z* $[M + Na]^+$ calculated for $C_{30}H_{33}F_3O_5Na^+$ 553.2172, found 553.2190.

4.1.9. General procedure for the synthesis of *WA19-WA23*.

To a stirred solution of **WA1-WA5** (1 equiv) in MeOH (5 mL) was added dropwise of HCl (10% aqueous solution, 2.0 mL). The mixture was refluxed at 70 °C for 1 h. After cooling to room temperature, the mixture was diluted with water (10 mL) and extracted with ethyl acetate (3 × 10 mL). The combined organic layer was dried with anhydrous Mg_2SO_4, filtered, and concentrated. The residue was purified by flash column chromatography over silica gel to obtain **WA19-WA23**.

*(E)-3-(3-(adamantan-1-yl)-4-hydroxyphenyl)-1-(2-hydroxyphenyl) prop-2-en-1-one (**WA19**)*. **WA1** was used to give **WA19**. Yellow solid, yield 35.3%, Mp: 180–183 °C. ^{1}H NMR (600 MHz, DMSO-d_6): δ 13.01 (s, 1H), 7.91–7.96 (m, 2H), 7.48–7.54 (m, 3H), 7.43 (dd, *J* = 2.0, 8.2 Hz, 1H), 7.04 (d, *J* = 8.2 Hz, 1H), 6.94–6.98 (m, 1H), 6.80 (d, *J* = 8.0 Hz, 1H), 2.15–2.16 (m, 9H), 1.72–1.74 (m, 6H). ^{13}C NMR (150 MHz, DMSO-d_6): δ 194.0, 178.9, 162.5, 160.1, 147.0, 136.7, 136.5, 131.1, 129.0, 125.8, 121.0, 119.5, 118.1, 117.6, 117.5, 39.0 (3C), 37.1 (3C), 36.5, 28.8 (3C). ESI-HRMS (–): *m/z* [M−H]- calculated for $C_{25}H_{25}O_3^-$ 373.1809, found 373.1808.

*(E)-3-(3-(adamantan-1-yl)-4-hydroxyphenyl)-1-(2-hydroxy-5-methylphenyl) prop-2-en-1-one (**WA20**)*. **WA2** was used to give **WA20**.Yellow solid, yield 37.4%, Mp: 174–175 °C. ^{1}H NMR (600 MHz, DMSO-d_6): δ 12.64 (s, 1H), 10.14 (s, 1H), 8.04 (d, *J* = 1.5 Hz, 1H), 7.82 (d, *J* = 15.6 Hz, 1H), 7.78 (d, *J* = 15.6 Hz, 1H), 7.70 (dd, *J* = 2.0, 8.4 Hz, 1H), 7.50 (d, *J* = 2.0 Hz, 1H), 7.36 (dd, *J* = 2.0, 8.4 Hz, 1H), 6.88 (dd, *J* = 1.5, 8.4 Hz, 2H), 2.33 (s, 3H), 2.02–2.14 (m, 9H), 1.73–1.76 (m, 6H). ^{13}C NMR (150 MHz, DMSO-d_6): δ 193.9, 160.4, 160.0, 146.8, 137.3, 136.6, 130.6, 129.5, 128.5, 128.3, 125.9, 120.7, 118.0, 117.8, 117.5, 40.6 (3C), 37.1 (3C), 36.8, 28.8 (3C), 20.5. ESI-HRMS (–): *m/z* $[M-H]^-$ calculated for $C_{26}H_{27}O_3^-$ 387.1966, found 387.1964.

*(E)-3-(3-(adamantan-1-yl)-4-hydroxyphenyl)-1-(5-chloro-2-hydroxyphenyl)prop-2-en-1-one (**WA21**)*. **WA3** was used to give **WA21**.Yellow solid, yield 34.1%, Mp: 185–187 °C. ^{1}H NMR (600 MHz, DMSO-d_6): δ 12.65 (s, 1H), 10.17 (s, 1H), 8.24 (d, *J* = 2.5 Hz, 1H), 7.82 (d, *J* = 15.6 Hz, 1H), 7.75 (d, *J* = 15.6 Hz, 1H), 7.69 (dd, *J* = 1.5, 8.3 Hz, 1H), 7.53 (dd, *J* = 2.5, 8.8 Hz, 1H), 7.50 (d, *J* = 1.5 Hz, 1H), 7.01 (d, *J* = 8.8 Hz, 1H), 6.88 (d, *J* = 8.3 Hz, 1H), 2.04–2.10 (m, 9H), 1.70–1.73 (m, 6H). ^{13}C NMR (150 MHz, DMSO-d_6): δ 192.8, 160.6, 160.2, 147.7, 136.7, 135.6, 129.9, 129.6, 128.9, 125.8, 123.2, 122.8, 120.1, 118.0, 117.5, 40.2 (3C), 37.1 (3C), 36.8, 28.8 (3C). ESI-HRMS (–): *m/z* $[M-H]^-$ calculated for $C_{25}H_{24}ClO_3^-$ 407.1419 and 409.1390, found 407.1417 and 409.1390.

*(E)-3-(3-(adamantan-1-yl)-4-hydroxyphenyl)-1-(2-hydroxy-5-methoxyphen-yl)prop-2-en-1-one (**WA22**)*. **WA4** was used to give **WA22**. Red solid, yield 44.1%, Mp: 194–197 °C. ^{1}H NMR (600 MHz, DMSO-d_6): δ 12.21 (s, 1H), 9.76 (s, 1H), 7.79 (d, *J* = 15.3 Hz, 1H), 7.58–7.61 (m, 2H), 7.49 (d, *J* = 1.5 Hz, 1H), 7.17–7.20 (m, 1H), 6.92–6.94 (m, 1H), 2.11–2.14 (m, 9H), 1.79–1.81 (m, 6H). ^{13}C NMR (150 MHz, DMSO-d_6): δ 193.6, 161.5, 158.8, 146.0, 139.1, 137.1, 129.3, 128.3, 127.9, 127.7, 127.5, 119.8, 118.3, 117.7, 114.7, 56.4, 40.5 (3C), 37.2 (3C), 37.0, 29.0 (3C). ESI-HRMS (–): *m/z* $[M-H]^-$ calculated for $C_{26}H_{27}O_4^-$ 403.1915, found 403.1911.

*(E)-3-[(3-(3-adamantan-1-yl)-4-hydroxyphenyl)acryloyl)]-4-hydroxybenzoic acid (**WA23**)*. **WA5** was used to give **WA23**. Yellow solid, yield 27.4%, Mp: 185–187 °C. ^{1}H NMR (600 MHz, DMSO-d_6): δ 10.20 (s, 1H), 8.53 (d, *J* = 2.0 Hz, 1H), 8.04 (dd, *J* = 2.0, 8.5 Hz, 1H), 7.79 (d, *J* = 15.6 Hz, 1H), 7.68 (d, *J* = 15.6 Hz, 1H), 7.64 (d, *J* = 1.5 Hz, 1H), 7.49 (d, *J* = 1.5 Hz, 1H), 7.07 (d, *J* = 8.5 Hz, 1H), 6.87 (d, *J* = 8.5 Hz, 1H), 2.04–2.10 (m, 9H), 1.70–1.73 (m, 6H). ^{13}C NMR (150 MHz, DMSO-d_6): δ 193.2, 167.1, 164.7, 160.1, 147.2, 136.7, 136.4, 132.6, 129.3, 128.7, 125.8, 122.2, 122.1, 118.7, 118.3, 117.6, 40.7 (3C), 37.0 (3C), 36.7, 28.8 (3C). ESI-HRMS (–): *m/z* $[M-H]^-$ calculated for $C_{26}H_{25}O_5^-$, 417.1707, found, 417.1700.

4.1.10. The synthesis of (E)-4-hydroxy-3-(3-(4-hydroxyphenyl)acryloyl)-benzoic acid (*WA24*).

To a solution of **6e** (1 mmol) and 4-hydroxybenzaldehyde **1a** (1.1 mmol) in MeOH (8 mL) was added 40% aqueous sodium hydroxide (2 mL). The reaction mixture was heated at 70 °C for 4–16 h. The progress of the reaction was monitored by TLC. After completion, the reaction mixture was cooled to 0 °C on an ice bath and acidified with 1 N HCl until pH = 5–6 was reached. The crude product was extracted with CH_2Cl_2 (50 mL × 3) and purified over silica gel column chromatography to give the corresponding chalcone AdAr **WA24**. Yellow solid, yield 25.8%, Mp: 194–196 °C. ^{1}H NMR (600 MHz, DMSO): δ 10.22 (s, 1H), 8.58 (d, *J* = 2.2 Hz, 1H), 8.06 (dd, 1H, *J* = 2.2, 8.6 Hz, 1H), 7.73–7.81 (m, 4H), 7.08 (d, *J* = 8.6 Hz, 1H), 6.86 (d, *J* = 8.6 Hz, 2H); ^{13}C NMR (150 MHz, $CDCl_3$): δ 193.3, 167.0, 164.9, 161.2, 146.4, 136.5, 132.6, 132.1, 128.9, 126.0, 122.2, 121.9, 118.9, 118.4, 116.4, 115.7. ESI-MS (–): *m/z* $[M-H]^-$ calculated for $C_{16}H_{11}O_5^-$, 283.0612, found, 283.0613.

4.2. Bioassay

4.2.1. Cell culture and transfection

All the human cancer cell lines (HepG2, A549, H460, H292) and two

human normal cell lines (LO2 and MRC-5) were purchased from the American type culture collection (ATCC, Shanghai China). HepG2, A549, H460, and H292 cancer cells were cultured in Dulbecco's modified Eagle medium (DMEM) supplemented with 10% fetal bovine serum (FBS), MCR-5 normal lung cells were cultured in minimum essential medium (MEM) supplemented with 10% FBS, LO2 normal hepatocytes cells were maintained in RPMI 1640 medium supplemented with 10% FBS and were cultured at 37 °C in a 5% CO_2 incubator. Cell transfections were carried out by using Lipofectamine 2000 (Invitrogen) according to the instructions of the manufacturer.

4.2.2. Cell proliferation assay

Cells were first plated onto a 96 well plate at a density of 5000 cells/100 μL per well and incubated overnight in an incubator at 37 °C. Following concentration gradients (2.5, 5, 10, 20, 40 and 80 μM) of compounds or DMSO treatment for 24 h, 20 μL MTT was added to each well, and cells were incubated in the dark for 4 h at 37 °C. The absorbance of the generated optical density (OD) was measured by a microplate reader (PerkinElmer, Waltham, MA) at 490 nm. Experiments were repeated three times. The results were analyzed by GraphPad Prism 6 software, La Jolla, CA.

4.2.3. Luciferase reporter gene assay

The experiments were performed as described previously. Briefly, HEK293T cells were co-transfected with the luciferase reporter plasmid pG5-Luc (40 ng) and the pBind-RARα-LBD (40 ng) or pBind-RXRα-LBD plasmid (40 ng). One day after transfection, the medium was replaced by a medium containing a respective ligand and/or a testing compound. After 12 h, cells were washed, lysed, and quantitated using the Dual-Luciferase Reporter Assay System (Thermo Fisher Scientific). Transfection and expression efficiency was normalized to Renilla luciferase activity.

4.2.4. Protein expression and purification

The expression and purification of the human RXRα-LBD (223–462) were performed by a standard method described previously [27].

4.2.5. Surface plasmon resonance (SPR) assay

The SPR assay studies were performed following a previously reported method [27].

4.2.6. Isothermal titration calorimetry (ITC) assay

The assay was conducted as described earlier [27].

4.2.7. Western blotting

Antibodies for RXRα (sc-553), PARP (sc-7150), and α-tubulin (sc-8035) were purchased from Santa Cruz Biotechnology; Antibody for IκBα (ab32518) was from Abcam; Antibodies for p-IKKα/β (#2078) was from Cell Signaling Technology. Goat and anti-rabbit secondary antibodies were obtained from Thermo Fisher Scientific, Inc. Briefly, protein samples were separated on a 10% SDS-polyacrylamide gel and transferred onto a polyvinylidene difluoride (PVDF) membrane. The membranes were blocked with 5% non-fat milk in 10 mM Tris-HCl (pH 8.0), 150 mM NaCl, 0.05% Tween 20 (TBST) buffer for 1 h at 37 °C. The membranes were washed with TBST three times, then incubated with rabbit polyclonal primary antibodies at 4 °C overnight. The membrane was then incubated with secondary antibodies (1:10,000) for 2 h at 37 °C. Lastly, an enhanced chemiluminescence kit (Advansta, Inc.) was used to analyze the membranes according to the instruction of the manufacturer.

4.2.8. Flow cytometry analysis of apoptosis

An Annexin V-FITC/PI dual staining assay was used to determine the percentage of apoptotic cells as described previously. H292 cells were plated in 6-well dishes. Following attachment, cells were treated with **WA15** for 12 h and harvested with trypsin at 37 °C without EDTA. After washing with 1 × PBS, the cells were resuspended in 250 mL binding buffer. Then the cell suspensions were stained with 5 μL PI and 5 μL Annexin V-fluorescein isothiocyanate solution (Yeasen, Inc.) and incubated at room temperature for 15 min in the dark. The cells were analyzed for the percentage undergoing apoptosis with a flow cytometer (ATTUNE NXT, Life tech, Inc.). All assays were performed in triplicate.

4.3. Molecular docking studies

The molecular docking studies were performed using Schrödinger software (Version 2017-1) [40]. The crystal structure of RXRα/RARα complex (PDB code: 3A9E) was downloaded from the RCSB protein data bank. The complex structure of RXRα containing LG100754 (PDB ID: 3A9E, Chain A) was used as a mode structure for molecular docking study. Protein RXRα was prepared with Protein Preparation Wizard panel as implemented in Maestro 10.5: water molecules were removed, missing hydrogens and residues were added, and the ionizable residues were protonated at the neutral pH. The glide grid center was setting according to the geometrical center of native ligand LG100754 and the grid size was 10 × 10 × 10 $Å^3$. The native ligand LG100754 and selected compounds including MX781, **WA11**, **WA15**, and **WA24** were prepared using the LigPrep suit of Schrödinger, which may produce an accurate prediction of the lowest energy 3D conformer of the docking molecule. Then they were bound to RXRα-LBD using Glide in extra precision (XP) mode. The MM/GBSA (Prime MMGBSA v3.000) was used to calculate the absolute binding free energy of complexes from the docking result [41]. Pymol (version 2.3.0, Open-Source PyMOL™ by Schrödinger) was used for making all the pictures of molecular docking [42].

Declaration of Competing Interest

The authors declare that they have no known competing financial interests or personal relationships that could have appeared to influence the work reported in this paper.

Acknowledgments

This work was supported by the Fundamental Research Funds for the Central Universities (No. 20720180051), the National Natural Science Foundation of China (No. 81773600 and 81772993), and the Natural Science Foundation of Fujian Province of China (No. 2018J01132).

The authors thank Cuiling Sun, Junjie Chen, and Rong Ding for assistance in using the Bruker AV 600 MHz spectrometer, Biacore T200 machine, VP-ITC titration calorimeter, and Q-Exactive mass spectrometer. They are from the Analysis and Measurement Center, School of Pharmaceutical Sciences, Xiamen University.

Appendix A. Supplementary material

Supplementary data to this article can be found online at https://doi.org/10.1016/j.bioorg.2021.104961.

References

[1] N.J. McKenna, Research Resources for Nuclear Receptor Signaling Pathways, Mol. Pharmacol. 90 (2) (2016) 153–159.
[2] S.A. Khan, J.P. Vanden Heuvel, Reviews: current topicsrole of nuclear receptors in the regulation of gene expression by dietary fatty acids (review), J. Nutritional Biochem. 14 (10) (2003) 554–567.
[3] T. Roszer, Transcriptional control of apoptotic cell clearance by macrophage nuclear receptors, Apoptosis 22 (2) (2017) 284–294.
[4] L. Rolf, J. Damoiseaux, R. Hupperts, I. Huitinga, J. Smolders, Network of nuclear receptor ligands in multiple sclerosis: Common pathways and interactions of sex-steroids, corticosteroids and vitamin D3-derived molecules, Autoimmun. Rev. 15 (9) (2016) 900–910.
[5] J.T. Moore, J.L. Collins, K.H. Pearce, The nuclear receptor superfamily and drug discovery, ChemMedChem 1 (5) (2006) 504–523.
[6] G.A. Francis, E. Fayard, F. Picard, J. Auwerx, Nuclear receptors and the control of metabolism, Annu. Rev. Physiol. 65 (2003) 261–311.

[7] A. Castrillo, P. Tontonoz, Nuclear receptors in macrophage biology: at the crossroads of lipid metabolism and inflammation, Annu. Rev. Cell Dev. Biol. 20 (2004) 455–480.
[8] N. Tanaka, T. Aoyama, S. Kimura, F.J. Gonzalez, Targeting nuclear receptors for the treatment of fatty liver disease, Pharmacol. Ther. 179 (2017) 142–157.
[9] K.N.N. Nicholas, F. Fitz, Radosveta Koldamova, Iliya Lefterov, Therapeutic targeting of nuclear receptors, liver X and retinoid X receptors, for Alzheimer's disease, J. Pharmacol. 176 (2019) 3599–3610.
[10] M. Moutinho, J.F. Codocedo, S.S. Puntambekar, G.E. Landreth, Nuclear Receptors as Therapeutic Targets for Neurodegenerative Diseases: Lost in Translation, Annu. Rev. Pharmacol. Toxicol. 59 (2019) 237–261.
[11] L. Zhang, Q. Wang, W. Liu, F. Liu, A. Ji, Y. Li, The Orphan Nuclear Receptor 4A1: A Potential New Therapeutic Target for Metabolic Diseases, J. Diabetes Res. 2018 (2018) 9363461.
[12] M.E. Kelly, H.M. Mohan, A.W. Baird, E.J. Ryan, D.C. Winter, Orphan Nuclear Receptors in Colorectal Cancer, Pathol. Oncol. Res. 24 (4) (2018) 815–819.
[13] A. Papi, M. Orlandi, Role of nuclear receptors in breast cancer stem cells, World J. Stem Cells 8 (3) (2016) 62–72.
[14] B.A. Porter, M.A. Ortiz, G. Bratslavsky, L. Kotula, Structure and Function of the Nuclear Receptor Superfamily and Current Targeted Therapies of Prostate Cancer, Cancers (Basel) 11 (12) (2019).
[15] D.A. Leach, S.M. Powell, C.L. Bevan, WOMEN IN CANCER THEMATIC REVIEW: New roles for nuclear receptors in prostate cancer, Endocr. Relat. Cancer 23 (11) (2016) T85–T108.
[16] T.B. Doan, J.D. Graham, C.L. Clarke, Emerging functional roles of nuclear receptors in breast cancer, J. Mol. Endocrinol. 58 (3) (2017) R169–R190.
[17] P. Huang, V. Chandra, F. Rastinejad, Structural overview of the nuclear receptor superfamily: insights into physiology and therapeutics, Annu. Rev. Physiol. 72 (2010) 247–272.
[18] D.H. Volle, Nuclear receptors as pharmacological targets, where are we now? Cell. Mol. Life Sci. 73 (20) (2016) 3777–3780.
[19] M. Moutinho, G.E. Landreth, Therapeutic potential of nuclear receptor agonists in Alzheimer's disease, J. Lipid Res. 58 (10) (2017) 1937–1949.
[20] A. Fischer, M. Smiesko, Ligand Pathways in Nuclear Receptors, J. Chem. Inf. Model. 59 (7) (2019) 3100–3109.
[21] V. Hiebl, A. Ladurner, S. Latkolik, V.M. Dirsch, Natural products as modulators of the nuclear receptors and metabolic sensors LXR, FXR and RXR, Biotechnol. Adv. 36 (6) (2018) 1657–1698.
[22] S.M.T. Vidyasagar Vuligonda, Roshantha A.S. Chandraratna, Enantioselective Syntheses of Potent Retinoid X Receptor Ligands: Differential Biological Activities of Individual Antipodes, J. Med. Chem. 44 (2001).
[23] C.E. Wagner, P.W. Jurutka, P.A. Marshall, T.L. Groy, A. van der Vaart, J.W. Ziller, J.K. Furmick, M.E. Graeber, E. Matro, B.V. Miguel, I.T. Tran, J. Kwon, J. N. Tedeschi, S. Moosavi, A. Danishyar, J.S. Philp, R.O. Khamees, J.N. Jackson, D. K. Grupe, S.L. Badshah, J.W. Hart, Modeling, synthesis and biological evaluation of potential retinoid X receptor (RXR) selective agonists: novel analogues of 4-[1-(3,5,5,8,8-pentamethyl-5,6,7,8-tetrahydro-2-naphthyl)ethynyl]benzoic acid (bexarotene), J. Med. Chem. 52 (19) (2009) 5950–5966.
[24] Z.Z. Ying Su, Ziwen Chen, Xu Dan, Weidong Zhang, Xiao-Kun Zhang, Recent Progress in the Design and Discovery of RXR Modulators Targeting Alternate Binding Sites of the Receptor, Curr. Top. Med. Chem. 17 (2017) 663–675.
[25] P.G. EfrenPerez Santın, Fabien Quillard, Harshal Khanwalkar, Fatima Rodrıguez-Barrios, Hinrich Gronemeyer, Angel R. de Lera, William Bourguet, Modulating Retinoid X Receptor with a Series of (E)-3-[4-Hydroxy-3-(3-alkoxy-5,5,8,8-tetramethyl-5,6,7,8-tetrahydronaphthalen-2-yl)phenyl]acrylic Acids and Their 4-Alkoxy Isomers, J. Med. Chem. 52 (2009).
[26] J.L. Fan Chen, Mingfeng Huang, Mengjie Hu, Su Ying, Xiao-kun Zhang, Identification of a New RXRα Antagonist Targeting the CoregulatorBinding Site, ACS Med. Chem. Lett. 5 (2014) 736–741.
[27] Z.S. Zhiping Zeng, Mingfeng Huang, Weidong Zhang, Jie Liu, Liqun Chen, Fan Chen, Yuqi Zhou, Jiacheng Lin, Fengyu Huang, Lin Xu, Zixing Zhuang, Shangjie Guo, Gulimiran Alitongbieke, Guobin Xie, Yang Xu, Bingzhen Lin, Xihua Cao, Ying Su, Xiao-kun Zhang, Hu Zhou, Nitrostyrene Derivatives Act as RXRa Ligands to Inhibit TNFa Activation of NF-kB, Cancer Res. 75(10) (2015) 2049–2060.
[28] S.C. Xin Wang, Huiyun Lin, Zhiqiang Yan, Fengyu Huang, Zhiping Zeng, Xiaokun Zhang, Ying Su, Discoveryof atorvastatin as a tetramer stabilizer of nuclear receptor RXRα through structure-based virtual screening, Bioorg. Chem. 85 (2019) 413–419.
[29] M.I. Dawson, Z. Xia, The retinoid X receptors and their ligands, BBA 1821 (1) (2012) 21–56.
[30] S. Perez-Rodriguez, M.A. Ortiz, R. Pereira, F. Rodriguez-Barrios, A.R. de Lera, F. J. Piedrafita, Highly twisted adamantyl arotinoids: synthesis, antiproliferative effects and RXR transactivation profiles, Eur. J. Med. Chem. 44 (6) (2009) 2434–2446.
[31] F.J.P.A.M.A. Ortiz, Mechanism of Action and Therapeutic Potential of Novel Adamantyl Retinoid-Relate, Current Cancer Therapy Rev. 2 (2006).
[32] R.A. Paula Lorenzo, Maria A. Ortiz, Susana Alvarez, F. Javier Piedrafita, Angel R. de Lera, Inhibition of IKB Kinase-✓ and Anticancer Activities of Novel Chalcone Adamantyl Arotinoids, J. Med. Chem. 51 (2008).
[33] M.I. Dawson, Z. Xia, T. Jiang, M. Ye, J.A. Fontana, L. Farhana, B. Patel, L.P. Xue, M. Bhuiyan, R. Pellicciari, A. Macchiarulo, R. Nuti, X.K. Zhang, Y.H. Han, L. Tautz, P.D. Hobbs, L. Jong, N. Waleh, W.R. Chao, G.S. Feng, Y. Pang, Y. Su, Adamantyl-substituted retinoid-derived molecules that interact with the orphan nuclear receptor small heterodimer partner: effects of replacing the 1-adamantyl or hydroxyl group on inhibition of cancer cell growth, induction of cancer cell apoptosis, and inhibition of SRC homology 2 domain-containing protein tyrosine phosphatase-2 activity, J. Med. Chem. 51 (18) (2008) 5650–5662.
[34] Z. Xia, R.G. Correa, J.K. Das, L. Farhana, D.J. Castro, J. Yu, R.G. Oshima, J. A. Fontana, J.C. Reed, M.I. Dawson, Analogues of orphan nuclear receptor small heterodimer partner ligand and apoptosis inducer (E)-4-[3-(1-adamantyl)-4-hydroxyphenyl]-3-chlorocinnamic acid. 2. Impact of 3-chloro group replacement on inhibition of proliferation and induction of apoptosis of leukemia and cancer cell lines, J. Med. Chem. 55 (1) (2012) 233–249.
[35] C. Zhuang, W. Zhang, C. Sheng, W. Zhang, C. Xing, Z. Miao, Chalcone: A Privileged Structure in Medicinal Chemistry, Chem. Rev. 117 (12) (2017) 7762–7810.
[36] H. Ur Rashid, Y. Xu, N. Ahmad, Y. Muhammad, L. Wang, Promising anti-inflammatory effects of chalcones via inhibition of cyclooxygenase, prostaglandin E 2, inducible NO synthase and nuclear factor κb activities, Bioorg. Chem. 87 (2019) 335–365.
[37] (a) P. Singh, A. Anand, V. Kumar, Recent developments in biological activities of chalcones: a mini review, Eur. J. Med. Chem. 85 (2014) 758–777;
(b) G. Wang, W. Liu, Y. Huang, Y. Li, Z. Peng, Design, synthesis, biological evaluation and molecular docking studies of new chalcone derivatives containing diaryl ether moiety as potential anticancer agents and tubulin polymerization inhibitors, Bioorg. Chem. 95 (2020), 103565;
(c) S. Burmaoglu, S. Ozcan, S. Balcioglu, M. Gencel, S.A.A. Noma, S. Essiz, B. Ates, O. Algul, Synthesis, biological evaluation and molecular docking studies of bischalcone derivatives as xanthine oxidase inhibitors and anticancer agents, Bioorg. Chem. 91 (2019), 103149.
[38] P. Lorenzo, M.A. Ortiz, R. Alvarez, F.J. Piedrafita, A.R. de Lera, Adamantyl arotinoids that inhibit IkappaB kinase alpha and IkappaB kinase beta, ChemMedChem 8 (7) (2013) 1184–1198.
[39] J. Garcia-Rodriguez, S. Perez-Rodriguez, M.A. Ortiz, R. Pereira, A.R. de Lera, F. J. Piedrafita, Inhibition of IkappaB kinase-beta and IkappaB kinase-alpha by heterocyclic adamantyl arotinoids, Bioorg. Med. Chem. 22 (4) (2014) 1285–1302.
[40] S.R. 2017-1:, Maestro, v., Schrödinger, LLC, New York, NY, (2016).
[41] M. Swanson, R.H. Henchman, J.A. McCammon, Revisiting free energy calculations: a theoretical connection to MM/PBSA and direct calculation of the association free energy, Biophys. J . 86 (1) (2004) 67–74.
[42] W. DeLano, The PyMOL Molecular Graphics System, DeLano Scientific, San Carlos, CA, USA, 2002, p. 2002.